processes

Article

Optimization Research on the Impact of Charging Load and Energy Efficiency of Pure Electric Vehicles

Huajian Xin [1], Zhejun Li [2], Feng Jiang [2], Qinglie Mo [2,*], Jie Hu [2] and Junming Zhou [2]

[1] School of Intelligent Manufacturing College, Guangxi Vocational & Technical Institute of Industry, Nanning 530001, China; 2019021246@gxgy.edu.cn
[2] School of Mechanical and Automotive Engineering, Guangxi University of Science and Technology, Liuzhou 545616, China; 18161019311@163.com (Z.L.); 100001086@gxust.edu.cn (F.J.); 2012031@gxust.edu.cn (J.H.); a13078027926@163.com (J.Z.)
* Correspondence: 100001683@gxust.edu.cn

Abstract: In this paper, the negative impact of the charging load generated by the disorderly charging scheme of large-scale pure electric vehicles on the operation performance of the power grid system and the problem of reducing its charging energy efficiency are studied and analyzed. First, based on Matlab 2022a simulation software and the Monte Carlo random sampling method, the probability density model of the factors affecting the charging load is constructed, and the total charging load of different quantities is simulated. Second, the IEEE33-node distribution network model is introduced to simulate the influence of charging load on the grid under different permeability schemes. Finally, the multi-objective genetic algorithm is used to optimize the charging cost and battery life. Taking the 20% permeability scheme as an example, the research results show that, compared with the disorderly charging scheme, the multi-objective optimization scheme reduces the peaking valley difference rate by 24.34%, the charging load power generation cost by 29.5%, and the charging cost by 23.9%. The power grid profit increased by 45.8%, and the research conclusion has practical significance for the energy efficiency optimization of pure electric vehicles.

Keywords: pure electric vehicles; Monte Carlo method; IEEE model; multi-objective genetic algorithm

Citation: Xin, H.; Li, Z.; Jiang, F.; Mo, Q.; Hu, J.; Zhou, J. Optimization Research on the Impact of Charging Load and Energy Efficiency of Pure Electric Vehicles. *Processes* **2024**, *12*, 2599. https://doi.org/10.3390/pr12112599

Academic Editor: Federica Raganati

Received: 19 September 2024
Revised: 26 October 2024
Accepted: 12 November 2024
Published: 19 November 2024

1. Introduction

Due to global economic growth driving industrialization and urbanization, climate change has heightened awareness of the atmosphere, with harmful gases produced by various industries continuing to increase. The world now faces an urgent and mandatory challenge to reduce air pollutants, making it imperative to curb pollution caused by gas emissions. Among these pollutants, NOx and N_2O have garnered significant attention [1]. Internal combustion engines and diesel engines are widely used in heavy vehicles, railway transportation, and marine applications. They use diesel fuel, which results in the emission of a significant amount of harmful substances in the exhaust [2,3]. According to the "2022 Annual Report on Environmental Statistics of China" released by the National Bureau of Statistics, the emissions within the scope of the pollution source survey in 2022 were reported as follows: sulfur dioxide emissions amounted to 2.435 million tons, nitrogen oxide emissions reached 8.957 million tons, and particulate matter emissions totaled 4.934 million tons. The emission of nitrogen oxide (NOx) from mobile sources amounts to 5.267 million tons, accounting for approximately 58.8% of the total nitrogen oxide emissions. Mobile sources can be broadly categorized into two main types: on-road mobile sources (motor vehicles) and non-road mobile sources. Notably, nearly 70% of nitrogen oxide (NOx) emissions are attributed to motor vehicle diesel engines [4].

For the aforementioned reasons, battery electric vehicles (BEVs), hybrid electric vehicles (HEVs), and fuel cell electric vehicles (FCEVs) have received considerable attention from automakers [5,6]. BEVs are crucial in reducing harmful emissions from traditional

fuel-powered vehicles. To address the challenges of fully electric vehicles, such as limited driving range, high battery costs, and long charging times, HEVs were introduced as an intermediate solution. HEVs combine batteries and electric motors with internal combustion engines, significantly improving vehicle fuel efficiency [7]. However, the ultimate goal remains the development of new energy, fully electric vehicles, which operate without fuel consumption and produce zero emissions. In order to promote ongoing societal development and achieve a green, low-carbon transition, the development of the new energy vehicle industry is a crucial aspect of building a sustainable transportation system. The widespread adoption of BEVs is instrumental in reducing dependence on fossil fuels and playing a significant role in environmental governance [8,9]. BEVs rely on only one energy source—the battery. BEVs need to be regularly connected to a power source to recharge, and this has been a primary subject of ongoing research [10,11]. Compared to traditional internal combustion engine vehicles, the main drawbacks of BEVs are their limited driving range and the high costs associated with purchasing and replacing batteries. Additionally, batteries pose other challenges, such as the need for an extensive charging infrastructure [7,12]. Presently, the primary performance metric for evaluating BEVs is the comprehensive driving range. However, optimizing vehicle charging efficiency has become a pressing research focus due to its dependence on factors such as battery energy density and cost [13]. The surge in charging load resulting from the large-scale adoption of BEVs presents challenges, as BEV charging is characterized by spatiotemporal randomness and unpredictability. This surge amplifies the strain on the power grid and complicates optimal scheduling, necessitating a quantitative assessment of the power grid's operational performance and methods to mitigate the impact of these loads [10]. Existing research on charging load scheduling schemes primarily focuses on shifting charging loads from peak periods to valley periods and is divided into centralized and distributed valley-filling control. The primary distinction between the two lies in the ownership of charging curve control; the former is managed by the grid, while the latter is set by BEV users themselves [14].

Currently, both domestic and international scholars have conducted extensive fundamental research on optimizing the charging efficiency of electric vehicles. The application of the Monte Carlo method in the analysis of EV charging loads is gaining increasing attention, particularly in the planning and management of charging infrastructure. By randomly sampling user charging behaviors, travel patterns, charging locations, and times, the Monte Carlo method can simulate charging demand under various conditions and can be used to predict charging loads within specific timeframes. For example, Yi et al. [15] studied the spatiotemporal distribution of EV charging load demand in a specific urban area of China using a Monte Carlo simulation. The results indicated significant spatiotemporal distribution characteristics of charging load demand across different functional zones, with noticeable differences between them. Furthermore, Xing et al. [16] utilized the Monte Carlo algorithm to develop a probabilistic distribution model for travel patterns and charging characteristics, predicting the load demand when large-scale EVs are integrated into the grid. Additionally, the stability of the power grid can be analyzed using the Monte Carlo method, as it can evaluate the impact of concentrated EV charging on the grid. For instance, Önder Polat et al. [17] employed Monte Carlo simulation to generate 1000 distinct charging load curves, each with a resolution of one minute, to accurately assess the impact of EVs. The study demonstrated that as the number of EVs increases, the load on distribution transformers rises, and voltage levels may drop to 0.76 pu., potentially leading to equipment failure for users. Additionally, to enhance the accuracy of the Monte Carlo-based charging load estimation, Bian et al. [18] proposed an improved Monte Carlo method, simulating the probability density models of factors influencing charging loads. The results showed that the accuracy of charging load estimation was improved with this enhancement.

The IEEE 33-bus distribution network system is a classical test system, which is commonly used to evaluate the performance of distribution networks, especially concerning the impact of electric vehicle charging loads. For example, Liu et al. [19] proposed a two-layer planning model to address the coordinated planning of distributed generation (*DG*)

and electric vehicle charging stations (*EVCS*). In their study, the researchers used the IEEE 33-bus test system to validate the effectiveness of the proposed model, and the results confirmed its validity. Similarly, Wang et al. [20] employed the IEEE 33-bus test system to implement the optimization of distributed energy resources. By comparing various charging strategies, they demonstrated that the proposed coordinated charging strategy could optimize the operation of distributed energy resources. However, an enhanced version of the IEEE 33-bus distribution test system has also been developed. Researchers introduced a new IEEE 33-bus distribution test system platform designed to correct some of the deficiencies in the Baran and Wu 33-bus distribution system and improve the test benchmark to better reflect real-world operational constraints [21]. The study shows that this platform can simulate unbalanced three-phase distribution systems. In addition, the system can accommodate various distribution system operations and planning studies, including system reconfiguration, and it is compatible with multiple power system analysis platforms [21].

In summary, the study of total charging load forecasting for pure electric vehicles is of significance for evaluating the performance of power grid operations. Due to its exceptional forecasting accuracy, the Monte Carlo sampling method has been favored by many researchers for large-scale pure electric vehicle total charging load predictions. Additionally, most studies on the impact of electric vehicle charging on the grid are based on using the IEEE framework as the research model, analyzing variations in load difference rate, node voltage deviation, and network loss rate. This study focuses on the large-scale deployment of pure EVs in a specific area of Liuzhou, Guangxi. First, the total charging load of EVs under an unordered electricity pricing scheme is determined using the Monte Carlo random sampling method. Then, based on the IEEE33 distribution network system, the impact on the grid under different EV penetration rates is assessed by examining indicators such as node voltage and load rate. Finally, a multi-objective optimization is conducted, targeting charging costs and battery life, resulting in a Pareto front for the two optimization goals. The results of this multi-objective optimization study have practical significance for enhancing the charging efficiency of pure electric vehicles and improving the operational performance of the power grid.

The structure of this paper is as follows:

Section 2 predicts and analyzes the total charging load by establishing the original load model of the distribution network and the total charging load model.

Section 3 analyzes the impact of charging load on the performance of power grid operations based on the IEEE 33-node distribution network system model.

Section 4 develops a multi-objective optimization model for charging costs and battery life and applies a genetic algorithm to optimize them for pure electric vehicles.

Section 5 concludes the paper.

2. Total Charge Load Forecasting and Impact Studies

Predicting the charging load of electric vehicles is a critical research area in power system management [22]. The objective of charging load forecasting is to reasonably estimate the charging demand of electric vehicles, assisting grid operators in power dispatch planning. This process helps to prevent grid overloads or localized power shortages, thereby ensuring stable grid operation [23,24]. This section establishes the original load model of the distribution network and the total charging load model, laying a foundation for charging load optimization in subsequent sections.

2.1. Establishment of Distribution Network Original Load Model

The study initially creates the original load curve of the power grid in the specified research area, which primarily depicts the distribution of electricity demand among all residents in the area. The original load data of the distribution network for a summer day in this area were gathered, with readings taken every 15 min, resulting in a total of 192 data sets. The real scenario and load curve are depicted in Figure 1. As illustrated in the figure,

the peak and valley distribution of the original load of the power grid on a summer day in this area is clearly visible. The time period between 12:00 and 20:00 represents the peak load region, while the period from 00:00 to 08:00 represents the valley load region.

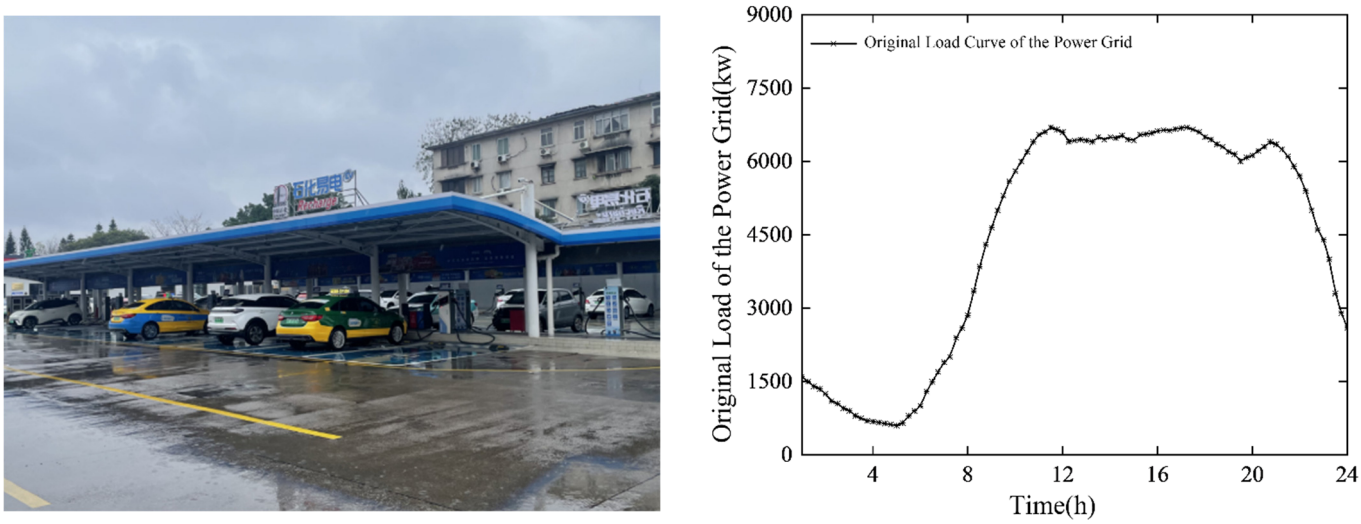

Figure 1. Distribution network load diagram in a study area.

2.2. Establishment of the Total Charging Load Model

The large-scale deployment of pure electric vehicles impacts the stability of the power grid, for example, by saving power during peak generation periods and supplying power to the grid during peak demand periods. Morsy Nour et al. [25] surmised that uncontrolled EV charging can severely affect the distribution network. Increased peak load demand may cause transformers and cables to overload, reducing their lifespan and increasing voltage drops. Additionally, single-phase chargers can introduce system imbalances, leading to higher power losses and greater harmonic distortion. This section first constructs probability density models for factors influencing charging load, such as charging power, daily driving mileage, initial charging time, and charging duration. Using the Monte Carlo random sampling method, the total charging load of various numbers of electric vehicles under a disordered charging scheme is simulated within the Matlab 2022a simulation environment.

(1) Charging power

The charging process of pure electric vehicles follows the conventional slow charging model, which depends on factors such as battery capacity, the power of the charging equipment, and the state of charge [25]. Generally, using a standard home charging station, it can take several hours, or even more than 10 h, to fully charge an electric vehicle's battery [26]. In this charging mode, there is a noticeable disparity between the charging start and end times, especially as the battery approaches full capacity. The charging speed gradually slows down to prevent overcharging or overheating, though this stage represents a small portion of the overall charging process. This variability requires efficient coordination between the charging equipment and the battery management system to ensure the safety and stability of the charging process [27]. Therefore, in the research process, simplifications were made by neglecting the impact of the start and end phases on the overall calculation. The time–probability rectangular coordinate system was simplified to a horizontal line, as shown in the simplified diagram in Figure 2.

(2) Mileage

At present, the ownership rate of pure electric vehicles is relatively low, primarily due to factors such as high acquisition costs, insufficient charging infrastructure, technological limitations, and low consumer acceptance. Although electric vehicles are relatively

economical in terms of operational costs and government policies provide some support, the high purchase price continues to deter many potential consumers. Furthermore, the lack of sufficient charging station coverage, especially in remote areas, intensifies concerns about the range and convenience of charging electric vehicles [28]. In addition, the current limitations in battery technology result in restricted driving range, causing consumers to question the practicality of electric vehicles [29]. Considering the current situation where the ownership of pure electric vehicles is still relatively low, this paper assumes that their driving habits are consistent with those of internal combustion engine vehicles. Referring to the results of the US Department of Transportation's National Household Travel Survey (NHTS) on household electric vehicles [30], the daily mileage is assumed to follow a log-normal distribution, with ($S \sim Log \sim N(\delta_s, \sigma_s^2)$), and its probability density function is shown as follows:

$$f_s(x) = \frac{1}{x\sigma_s\sqrt{2\pi}} \exp\left(-\frac{(\ln x - \delta_s)^2}{2\sigma_s^2}\right) \quad (1)$$

In the equation, δ_s represents the expected daily mileage of pure electric vehicles, σ_s represents the variance, and x is the specific driving distance in kilometers, where δ_s = 4.0 and σ_s = 0.88. Using a case study of 1000 pure electric vehicles, the probability distribution of daily mileage in this region can be obtained, as shown in Figure 3. Most of the daily driving mileage for pure electric vehicles is concentrated in the range of 0–60 km, with the primary usage being daily commuting to and from work.

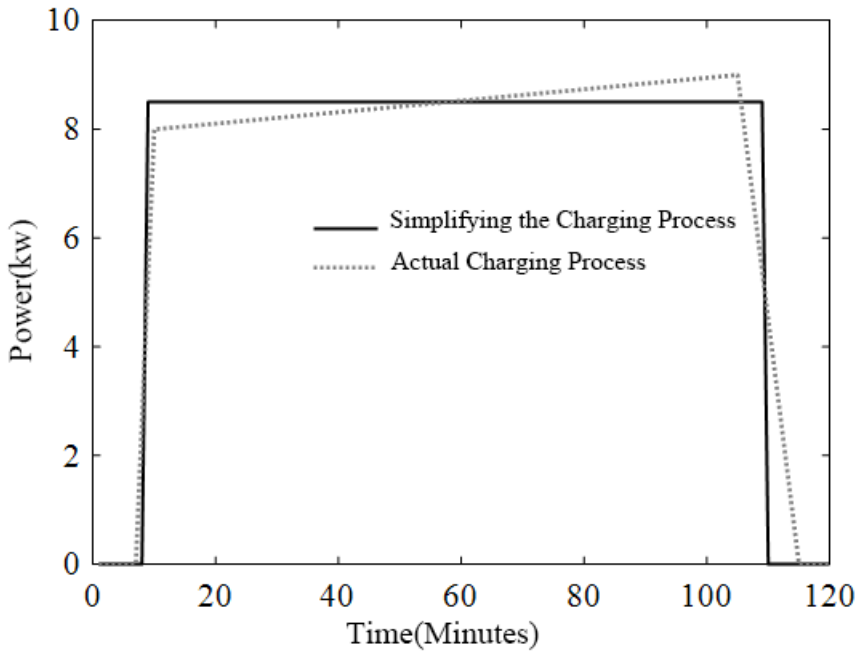

Figure 2. Simplified schematic diagram of charging power for pure electric vehicles.

(3) The time of initial charging

The return time of pure electric vehicles, which corresponds to the start of charging time t_0, follows a normal distribution, with $t_0 : N(\delta_{t_0}, \sigma_{t_0}^2)$. Its probability density function is shown as follows:

$$f_{t_0}(x) = \begin{cases} \frac{1}{\sigma_{t_0}\sqrt{2\pi}} \exp\left(-\frac{(x-\delta_{t_0})^2}{2\sigma_{t_0}^2}\right) & \delta_{t_0} - 12 < x < 24 \\ \frac{1}{\sigma_{t_0}\sqrt{2\pi}} \exp\left(-\frac{(x+24-\delta_{t_0})^2}{2\sigma_{t_0}^2}\right) & 0 < x < \delta_{t_0} - 12 \end{cases} \quad (2)$$

In the equation, δ_{t_0} and σ_{t_0} are also derived from statistical data on the daily driving behavior of users in the region, with values of 19.6 and 3.4, respectively. Therefore, the

probability distribution of the charging start time can be obtained, as shown in Figure 4. The charging start time for most pure electric vehicles returning home is concentrated between 18:00 and 21:00. During this period, a large number of electric vehicle users connect directly to the grid for charging, leading to peak load demand, which can affect the stability of power grid generation.

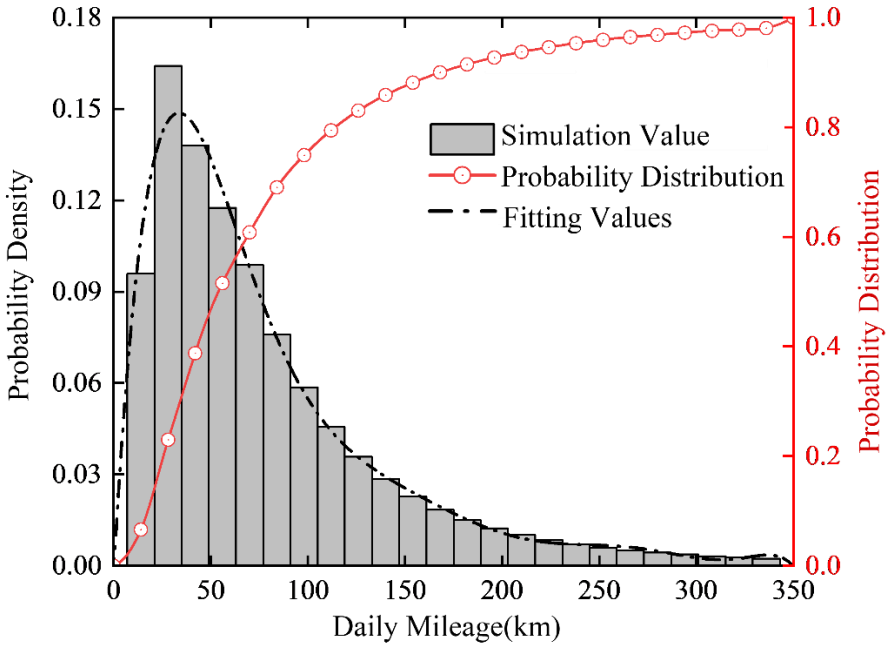

Figure 3. Probability distribution of daily mileage of pure electric vehicles.

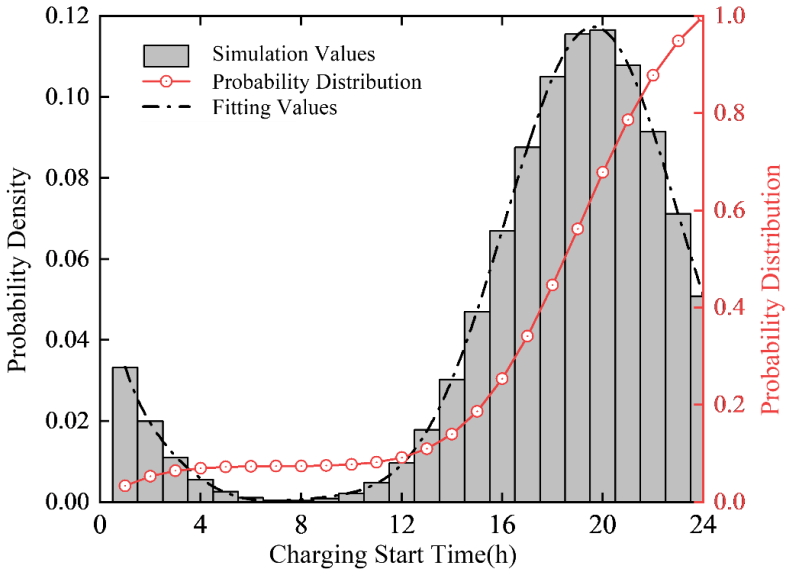

Figure 4. Probability distribution of the initial charging moment of a pure electric vehicle.

(4) Charging time

The charging duration (t) is typically determined by factors such as daily driving distance in kilometers (x), energy consumption per 100 km (E_d), required charging amount (D_n), and battery capacity (B). First, the initial state of charge at the beginning of the charging time ($SOC_{pre.t}$) is defined as follows.

$$SOC_{\mathrm{pre.t}} = 1 - \frac{x \times E_{\mathrm{d}}}{100 \times B} \tag{3}$$

Using the charging power (P_c) and a charging constant (K), the time required to reach a fully charged state (t) can be calculated as follows.Differences in vehicle size, the number of battery packs, and battery conditions can be considered. For example, when comparing smaller electric vehicles, such as the Baojun E-Series and Wuling Mini Series, which have a high market share in the region, to larger electric vehicles like the BYD Han, which have a smaller market share, it can be seen that the former has a battery capacity of only 31.4 kW·h and energy consumption of about 9 kW·h per 100 km, while the latter has a battery capacity of 86.0 kW·h and energy consumption of about 16 kW·h per 100 km. To minimize relative error, this study assumes that all vehicles have an average battery capacity of 45 kW·h and an energy consumption of 10.5 kW·h per 100 km. A standard AC charging power of 7 kW/h is used, and it is uniformly stipulated that all simulated vehicles have batteries of the same condition to ensure the reasonableness of the subsequent optimization process. The simulation analysis provides a specific distribution diagram of the required charging amount and charging time for electric vehicles after daily driving, as shown in Figure 5. From the figure, it can be seen that the required charging amount is mostly within 0–15 kW·h, and the required charging time is mainly distributed within 0–2 h.

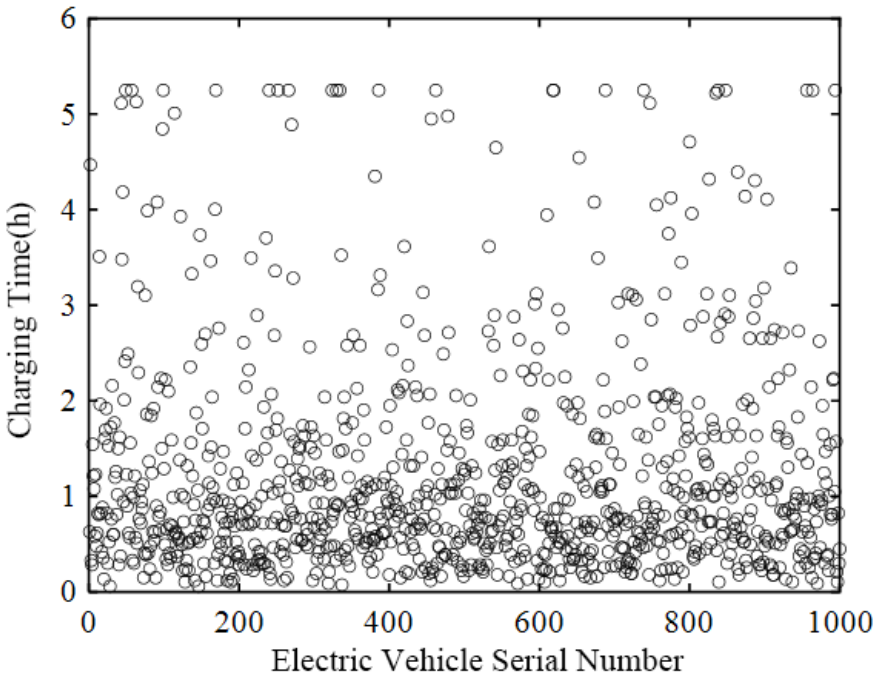

Figure 5. Probability distribution of charging time for pure electric vehicles.

2.3. Simulation Analysis of Total Charging Load

In this section, we utilize the Monte Carlo random sampling method to model the total charging load based on the factors mentioned earlier. The simulation process entails initializing simulation parameters, randomly generating values for daily driving distance and initial charging time, obtaining random values for the required charging amount and charging time, simulating the charging load for each electric vehicle, and integrating it into the original load curve of the power grid. The process then evaluates whether all charging events in the current simulation group are complete and ultimately calculates the total charging load [31]. For a more detailed explanation of the process for calculating the total charging load, please refer to Figure 6. First, determine the total number (n) of pure electric vehicles in the region and their charging methods. Then, randomly sample the battery capacity and charging power of the electric vehicles. Next, randomly select the daily mileage and the charging time of the electric vehicles. Finally, calculate the charging

duration and the required energy to fully charge. Afterward, evaluate whether the specified conditions have been met and ultimately obtain the results.

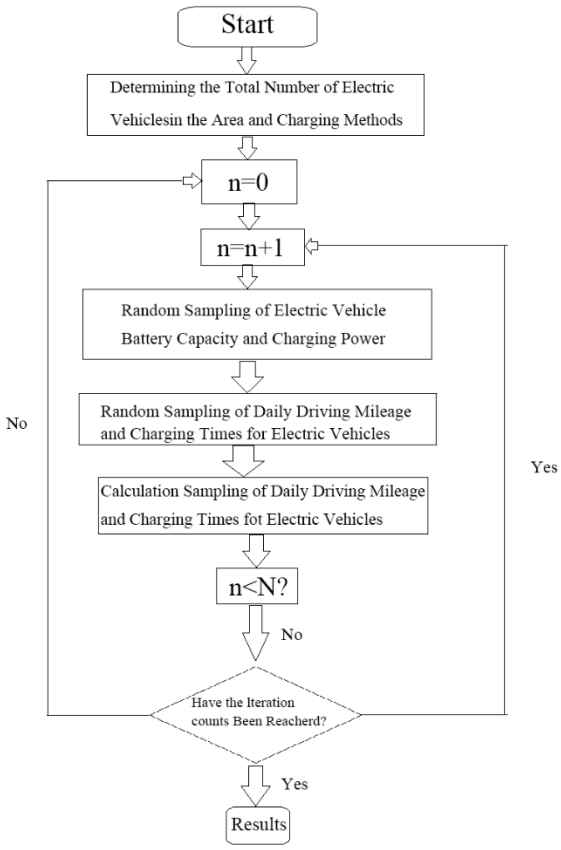

Figure 6. Flow chart of total charging load calculation.

Following the utilization of a Matlab 2022a simulation program, the total charging load for electric vehicles was determined under three distinct quantity scenarios, as depicted in Figure 7. The peak charging loads for the three scenarios coincide at 20:00 and amount to 1784.4 kW, 1220.7 kW, and 615.5 kW, respectively. This timeframe aligns with the peak load zone of the distribution network in conjunction with the original grid load. It is apparent that the incorporation of electric vehicles into the grid will unavoidably escalate the peak load, thus impacting the stability of power generation within the grid.

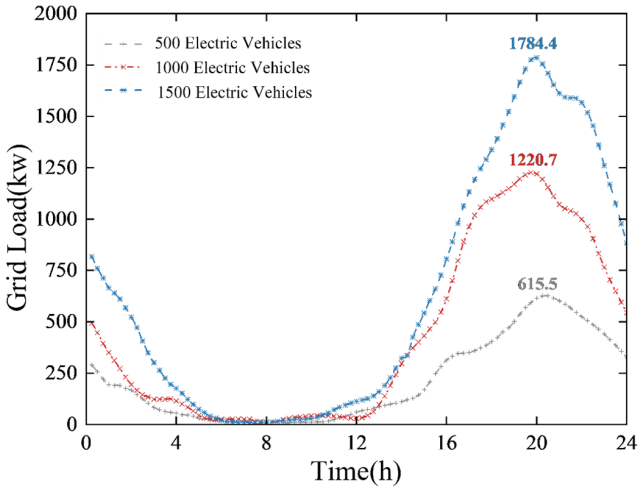

Figure 7. Diagram of the total charging load curve of the three BEV quantity schemes.

3. Analysis of the Impact of Charging Loads on Grid Operation Performance

The impact of charging loads on the operational performance of power grids has become a critical issue in current power system research, particularly with the increasing penetration of electric vehicles [31,32]. The uncertainty and volatility of charging loads may result in voltage deviations, line overloads, and increased system losses, which in turn affect the safe and stable operation of the distribution network. To study the impact of disordered charging schemes on the power grid, this section introduces the IEEE 33-bus distribution network system. By setting up three electric vehicle penetration rate scenarios, the variations in power grid performance indicators, such as node voltage, network losses, and load rate, are analyzed under each scenario.

3.1. Establishment of the IEEE 33-Node Distribution Network System Model

The IEEE 33-bus distribution network model is a standard test system widely used in power system research. In the initial phase, a smaller-scale system allows us to observe and analyze the performance of the proposed method more clearly and in a controlled manner, ensuring that the method's effectiveness is accurately evaluated under smaller-scale conditions. This section analyzes the variations in grid performance indicators—such as node voltage, network losses, and load rate—under different scenarios by setting three electric vehicle penetration rates. In existing research, the IEEE 33-bus model is commonly applied for analyzing grid operational performance [33], and its topology and functional divisions are illustrated in Figure 8.

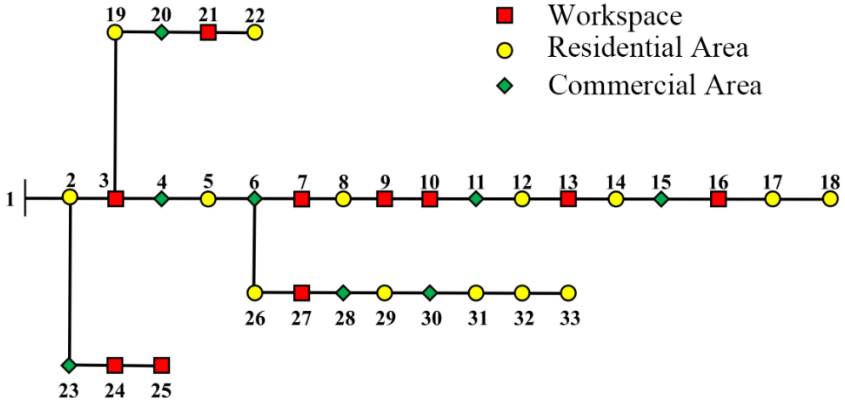

Figure 8. IEEE33 node system topology of the distribution network.

3.2. Analysis of the Impact of Peak Load Levels

To more accurately quantitatively describe the degree of grid impact, it is assumed that there are 5000 motorized vehicles in the study area, in which the pure electric vehicle penetration rate scenarios are set at 10%, 20%, and 30%, defined as the ratio of the number of pure electric vehicles to the total number of motorized vehicles. The indicators for evaluating the operational performance of the grid include the grid peak-to-valley difference rate σ and the load rate ρ. The former refers to the utilization of the grid load in the region, and the larger the value is, the lower the degree of utilization of the grid load is, which indicates that more load-shaving and valley-filling measures are needed in the region. The latter is defined as the ratio of the peak load P_{peak} to the average load P_{avg} in a specified period; the closer the value is to 1, the higher the utilization of the charging infrastructure in the region and the better the economic performance of the grid power generation cost [34]. The specific calculation formula is shown below:

$$\sigma = \frac{\max P_{\text{peak}} - \min P_{\text{vally}}}{\max P_{\text{peak}}} \tag{4}$$

$$\rho = \frac{P_{\text{avg}}}{\max P_{\text{peak}}} \tag{5}$$

Based on the detailed explanation of the peak-to-valley load difference ratio (σ) and the load factor (ρ), a quantitative analysis of the grid under three different penetration rate scenarios for uncoordinated charging schemes can be conducted, as shown in Table 1. As indicated in the table, compared to the original grid load, the charging load under different penetration rates increases the peak-to-valley load difference ratio while reducing the load factor.

Table 1. The impact of different permeability rates on grid load.

Penetration Rate/%	Peak Load/kW	Valley Load/kW	Peak-to-Valley Difference/kW	Peak-to-Valley Spread/%	Load Factor/%
0	6679.8	598.6	6081.2	91.03	65.16
10	7060.0	631.1	6428.9	91.06	64.71
20	7718.7	645.0	7073.7	91.64	61.98
30	8054.1	674.9	7379.2	91.62	61.86

3.3. Analysis of the Impact of Node Voltage

Voltage simulations for each node are conducted using the IEEE 33-bus distribution network model, with a voltage reference value of 12.6 kV. According to the standards specified in GB/T12305-2008 [35], a node voltage deviation within the range of [0.93 pu, 1.07 pu] is considered compliant. The voltage distribution for each node under three different penetration scenarios is determined using the forward-backward sweep load flow calculation method, as illustrated in Figure 9. The figure demonstrates that in all three scenarios, the lowest voltages occur at Node 18 during the 20:00 time period, with values of 0.924 pu, 0.912 pu, and 0.896 pu, all of which fall outside the acceptable voltage range. Node 18 is situated at the far end of the system, at a significant distance from the primary power source at Node 1, resulting in the lowest node voltage. Without appropriate optimization measures, the increasing charging load of the grid will continue to escalate the generation costs, significantly impacting the charging efficiency and economic feasibility of pure electric vehicles.

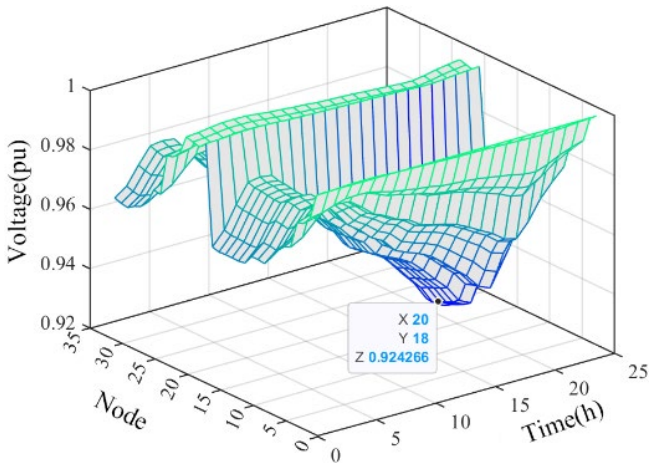

10%

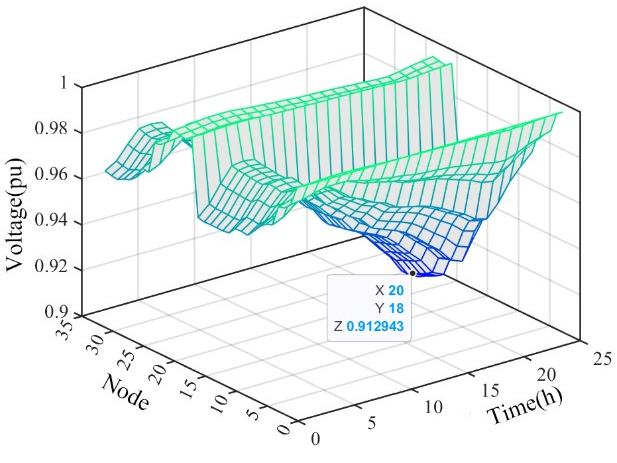

20%

Figure 9. *Cont.*

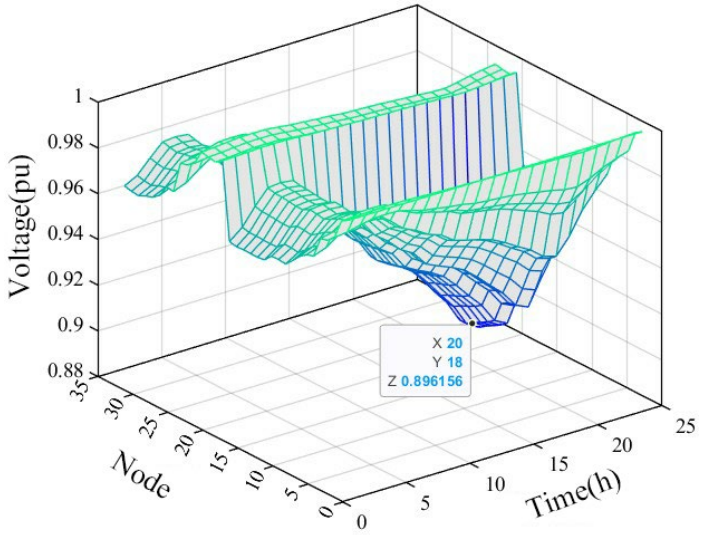

30%

Figure 9. Nodal voltages for the three penetration rate scenarios.

4. Research on Charging Energy Efficiency Optimization

Research on the optimization of charging energy efficiency has become a significant topic in the current energy sector, especially in the context of the rapid proliferation of EVs. The widespread adoption of electric vehicles has not only transformed the transportation sector but has also posed higher demands on the stability and energy efficiency of power systems. In this process, optimizing charging energy efficiency can reduce the charging costs for electric vehicle users, alleviate the load pressure on the power grid, and improve overall energy utilization efficiency [36]. This section utilizes a genetic algorithm to optimize the charging cost of pure electric vehicles and battery lifespan. These two objectives are simultaneously integrated into the charging curve $P_{EV}(t,n)$ for multi-objective optimization, resulting in the Pareto solution set under different charging curve scenarios.

4.1. Establishment of a Multi-Objective Optimization Model Based on Charging Costs and Battery Life

(1) Optimization Objective Function for Charging Costs

The charging cost optimization objective function for pure EVs plays a critical role in their operation and management [37]. First, the charging cost optimization objective function helps users choose the optimal charging time by analyzing electricity price fluctuations, charging periods, and demand. During peak periods, electricity prices are typically higher, while they are relatively lower during off-peak times. Second, the optimization objective function also takes into account the pricing standards and service quality of different charging stations. By comparing the prices and locations of various charging stations, users can select the most cost-effective charging solution. This flexibility not only improves the user experience but also promotes the rational layout of the charging infrastructure [38]. Within the vehicle-to-grid system, the distributed valley-filling control of pure electric vehicles enhances charging load efficiency by regulating the charging curve $P_{EV}(t,n)$. This study undertakes an examination and analysis focusing on two optimization objectives: charging cost and battery lifespan. To begin, an expression for optimizing charging costs is articulated through the development of an optimal time-of-use pricing scheme based on charging time (t) and charging power (P). This pricing scheme is closely linked to the valley-filling load across various penetration scenarios. Utilizing Matlab 2022a simulation, the valley-filling load for different scenarios is obtained, as depicted in Figure 10. This study then formulates the appropriate final pricing scheme based on the 20% penetration scenario.

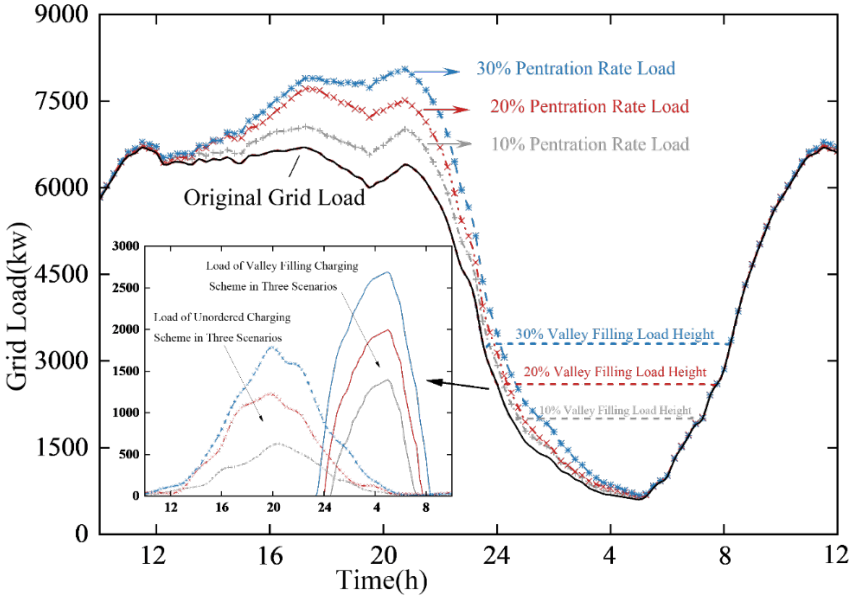

Figure 10. Load shaving conditions for three penetration rate scenarios.

The above figure shows that the valley-filling load under the 20% penetration scenario is 2.6×10^3 kW. Therefore, the corresponding pricing scheme and objective function can be further developed.

$$f_{\text{ele-v}}(t, P) = \frac{P^*_{\text{EV.sum}}(t)}{P_{\text{v-f}} \times N} \times C\left(P / \frac{P^*_{\text{EV.sum}}(t)}{P_{\text{v-f}} \times N}\right) \tag{6}$$

From the above equation, it can be inferred that the optimal time-of-use pricing under different penetration rates is primarily related to the optimal valley-filling height P_{v-f} of grid charging and the combination of charging curves for all electric vehicles $P^*_{EV.sum}(t)$. Figure 11 presents a diagram of optimal pricing as a function of time t and power P.

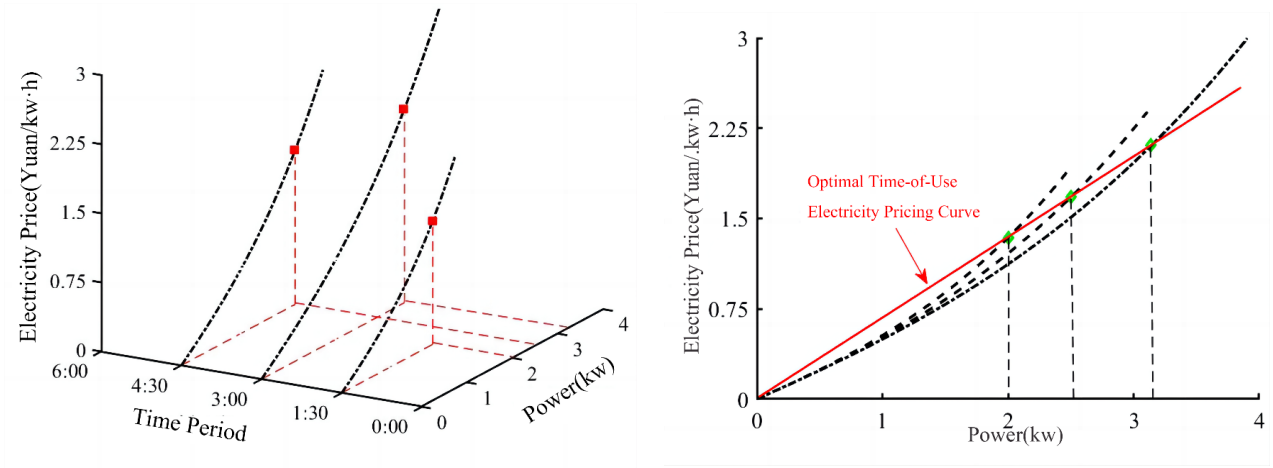

Overall Perspective Side Perspective

Figure 11. Optimal time-of-use pricing scheme.

In Figure 11, the side view indicates that the pricing scheme is represented by the red solid line. It is a convex function with respect to variations in time and power, which means that a minimum pricing scheme exists at specific time and power values. The core of the charging pricing scheme lies in minimizing charging costs while ensuring the battery is fully charged.

Based on the optimal time-of-use pricing scheme, a cost-minimization objective function for charging is constructed:

$$\min_{P_{\mathrm{EV}}(t,n)} F_{\mathrm{EV}}(n) = \int_{t_{\mathrm{ev,e}}}^{t_{\mathrm{ev,s}}} f_{\mathrm{ele}}(t, P_{\mathrm{EV}}(t,n))\mathrm{d}t \tag{7}$$

(2) Battery Life Optimization Objective Function

The optimization objectives for the charging efficiency of pure electric vehicles typically include battery lifespan and charging costs. The battery is one of the most critical components of an electric vehicle, and its state of health directly affects the long-term performance of the vehicle [39]. The charging and discharging cycles, charging speed, and the amount of charge all impact the battery's lifespan. Frequent use of fast charging increases the battery's heat, leading to the gradual degradation of its chemical structure, ultimately shortening its lifespan [40]. The primary objective of optimizing battery lifespan is to provide a quantitative description of the battery capacity degradation process [41]. In current research, the description of battery capacity degradation primarily focuses on the consumption of lithium ions by the solid electrolyte interphase (SEI) film. The formation of the SEI layer is closely related to chemical reactions and ion concentrations, both of which significantly impact the battery's safety and performance. At elevated temperatures, the solubility of the SEI layer increases, potentially leading to the formation of lithium crystals that are impermeable to Li+, thus raising the impedance of the negative electrode [42]. Presently, research on battery capacity degradation predominantly focuses on the consumption of lithium ions by the SEI film. This paper initially establishes an experimental platform for the cycle life of lithium-ion batteries. Using electrochemical theory, the internal mechanism of the P2D model is simulated and analyzed using Comsol simulation software (https://www.comsol.com/). Additionally, Figure 12 illustrates the schematic diagram of the battery cycle life experimental setup.

A simulation analysis of the five primary mechanism equations and side reaction equations of the P2D model of a lithium-ion battery is conducted under a 1C charge-discharge rate and at 25 °C. Table 2 presents the simulation parameters of the P2D model.

Table 2. P2D model simulation parameters.

Parameter Name	Cathode	Anodal	Distant (Socially Aloof)	Unit (of Measure)
Active Materials	**Plumbago**	**NCA (LiNi0.8Co0.15Al0.05O2)**	**LiPF6**	**-**
A		0.0846		m^2
L	5.5×10^{-5}	4×10^{-5}	3×10^{-5}	m
R_p	2.5×10^{-6}	2.5×10^{-7}	-	m
$\varepsilon_s^{\mathrm{brugg}}$	0.384	0.42	-	-
$\varepsilon_l^{\mathrm{brugg}}$	0.444	0.41	-	-
Brugg		1.5		-
c_s	30,555	48,000	-	mol/m^3
c_l		1200		mol/m^3
D_s	3.8×10^{-15}	1.0×10^{-15}	-	m^2/s
D_l	7.6×10^{-10}	7.6×10^{-10}	7.6×10^{-10}	m^2/s
κ^{eff}	100	-	100	S/m
U_{SEI}^{ref}	0.4	-	-	-
t_+		0.365		-
R		8.314		$J\cdot(mol^{-1}K^{-1})$
T		298.15		K
F		9.6486×10^4		C/mol
a_a	0.5	0.5	-	-
a_c	0.5	0.5	-	-

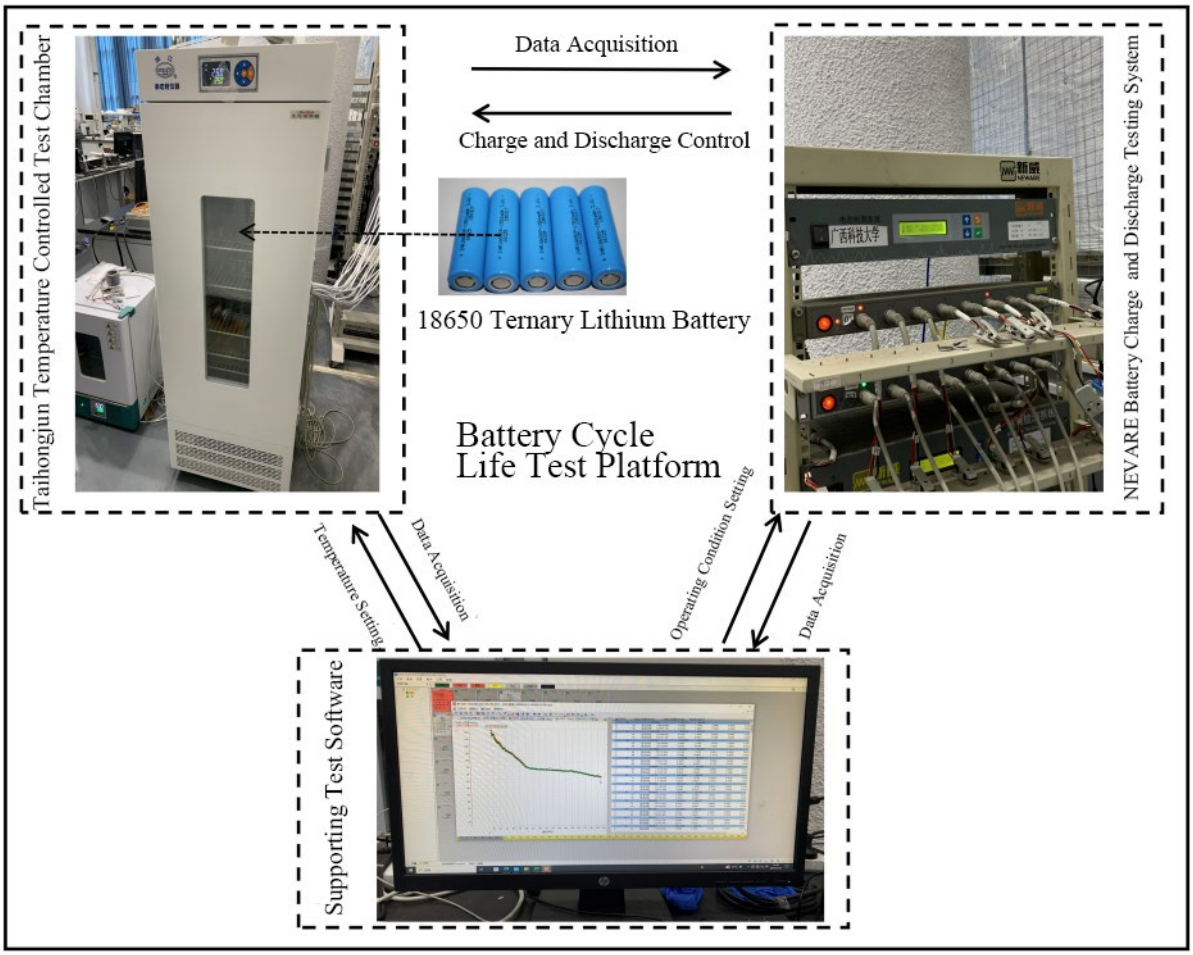

Figure 12. Schematic diagram of battery cycle life testing equipment.

To verify the accuracy of the parameters in Table 2, a validation analysis was performed using COMSOL software and experimental results. Under a 1C simulation condition, the open-circuit voltages of the positive and negative electrodes of the P2D model and the simulation results of the charging voltage at different charge rates were recorded. Finally, the experimental voltage was compared with the simulated voltage for verification, and the results are shown in the Figure 13 below.

As shown in Figure 13, the experimental values and simulation values are generally consistent, with small deviations occurring at certain time points. The primary reason for this is the discrepancy between some parameters of the P2D model and the experimental values, as well as the fact that the open-circuit voltage is calculated based on simulation data. However, the overall error is within an acceptable range, indicating that the accuracy of the P2D model meets the requirements, providing a solid foundation for subsequent battery cycle life experiments.

Figure 14 illustrates that the rapid growth of the SEI film predominantly occurs in the charging region.

From Figure 14, it can be observed that the rapid growth region of the SEI film is primarily concentrated in the charging zone during the simulation period of 2000–4000 s, with the current density reaching its peak as the SOC increases. Therefore, in the subsequent P2D model simulation analysis, five time points-2000 s, 2500 s, 3000 s, 3500 s, and 4000 s-will be selected from the charging region for detailed analysis.

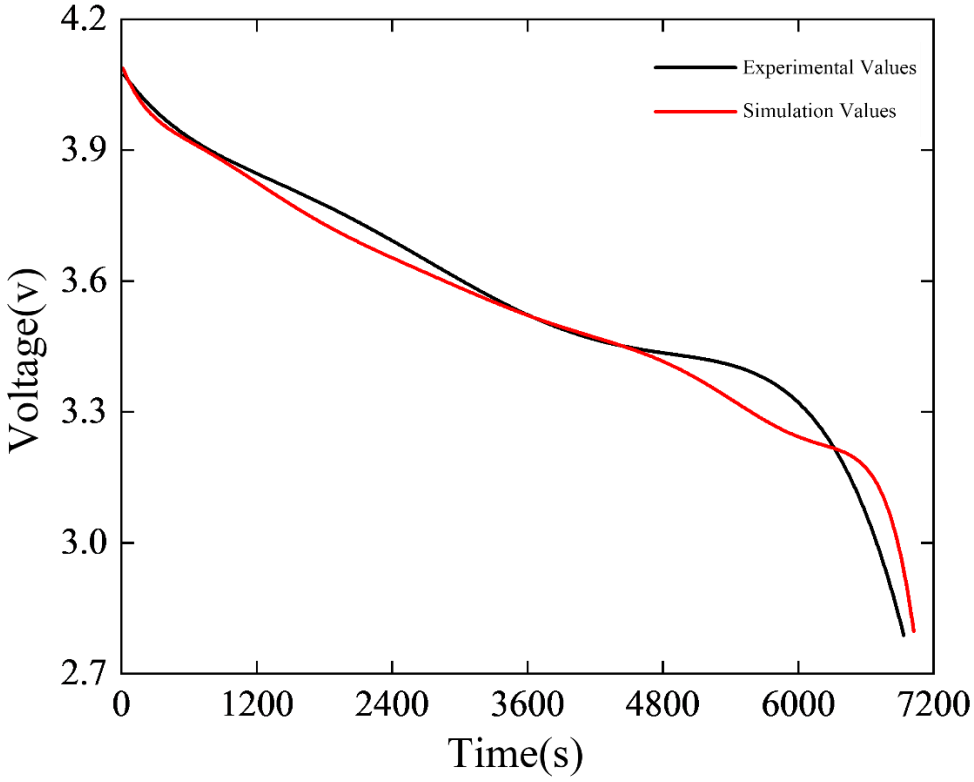

Figure 13. Comparison of P2D experiment and simulation data.

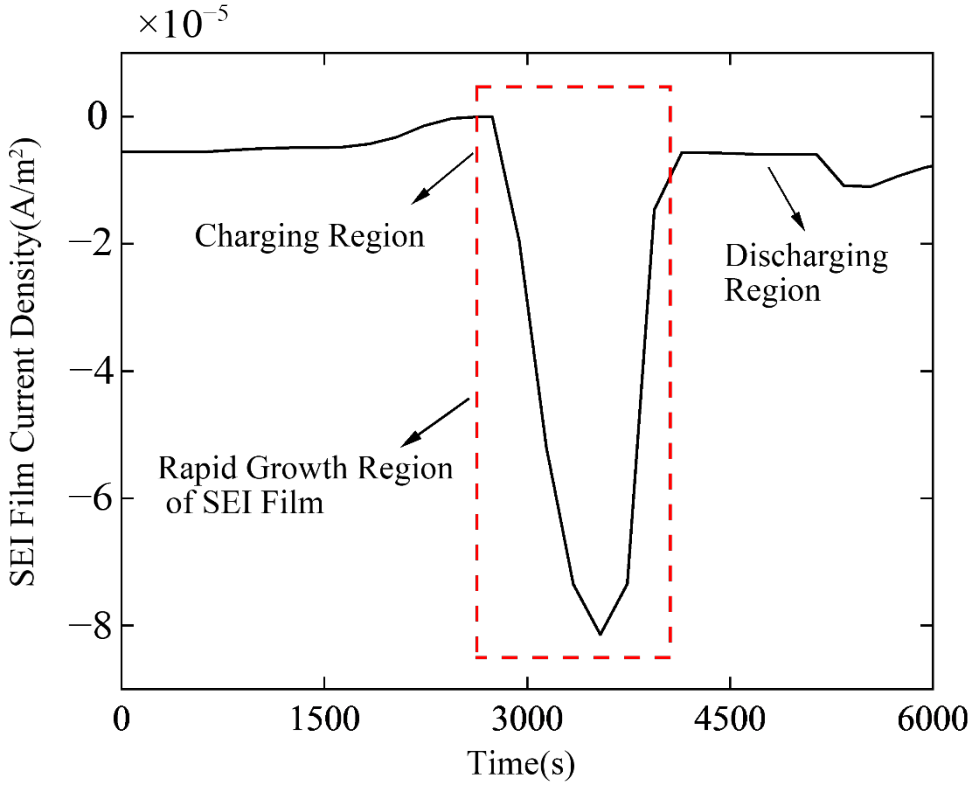

Figure 14. SEI film growth area under simulated working conditions.

(1) Primary and Secondary Reaction Current Densities

From Figures 15 and 16, the distribution of the primary and secondary reaction equations on the graphite material of the anode under constant current charging conditions

can be observed. The primary reaction current density shows irregular patterns. As shown in Figure 15, at the time points of 3000 s and 4000 s, the current density at the right end (near the separator) is lower than that at the left end (near the current separator), while the opposite is true at 2000 s, 2500 s, and 3500 s. In contrast to the primary reaction current density, the secondary reaction current density exhibits a certain regularity. As shown in Figure 16, at all five time points, the current density at the right end is greater than at the left. Additionally, as the charging time progresses and the SOC increases, the secondary reaction current density at all locations also increases correspondingly.

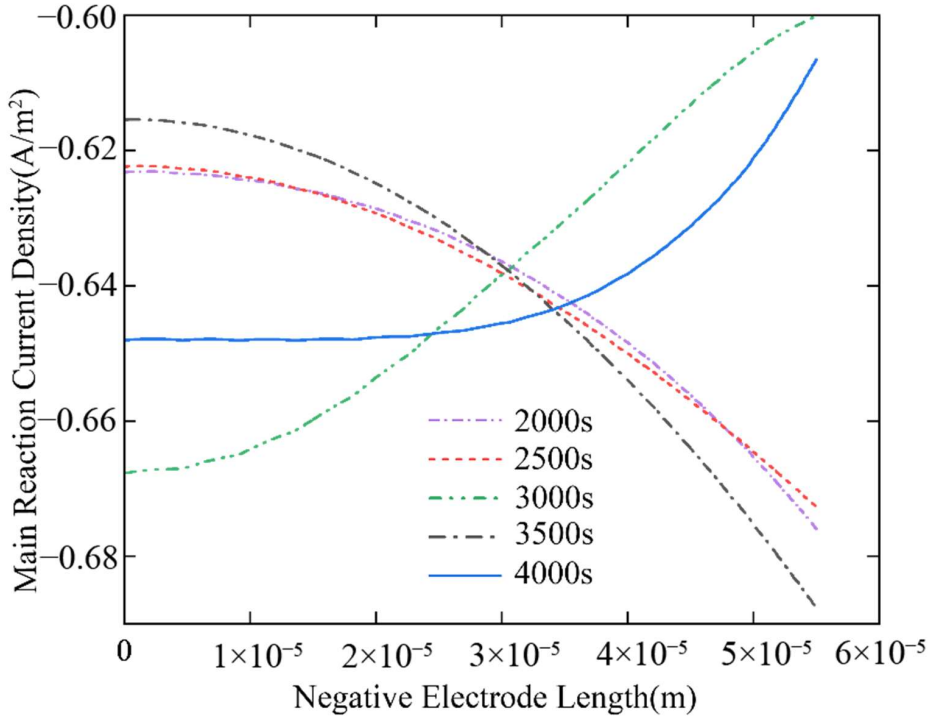

Figure 15. Current density diagram of the main reaction equation.

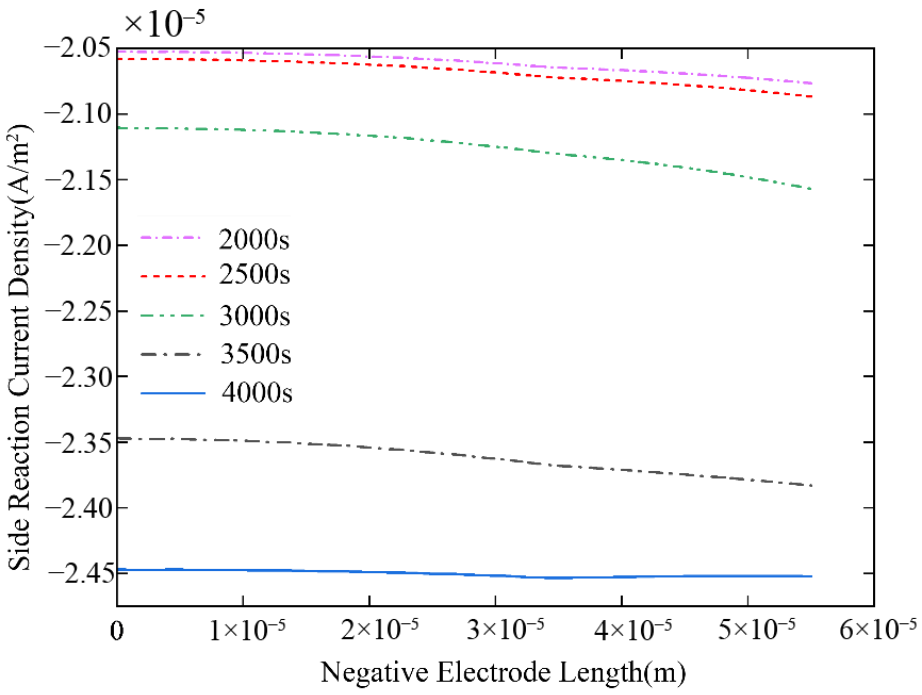

Figure 16. Current density diagram of side reaction equation.

(2) Liquid-phase Species and Potential Distribution

Figure 17 illustrates the distribution of liquid-phase lithium-ion concentration over simulation time, while Figure 18 shows the distribution of liquid-phase lithium-ion potential over simulation time. From the trends in lithium-ion concentration and potential shown in both figures, it can be observed that as time increases, both the concentration and potential increase accordingly. In the anode, separator, and cathode regions, the lithium-ion concentration and potential are higher at the right end than at the left, and they maintain a linear trend in the separator region. In addition, the distribution of liquid-phase lithium-ion concentration and potential exhibits strong regularity, laying a theoretical foundation for future simplification studies of the P2D model.

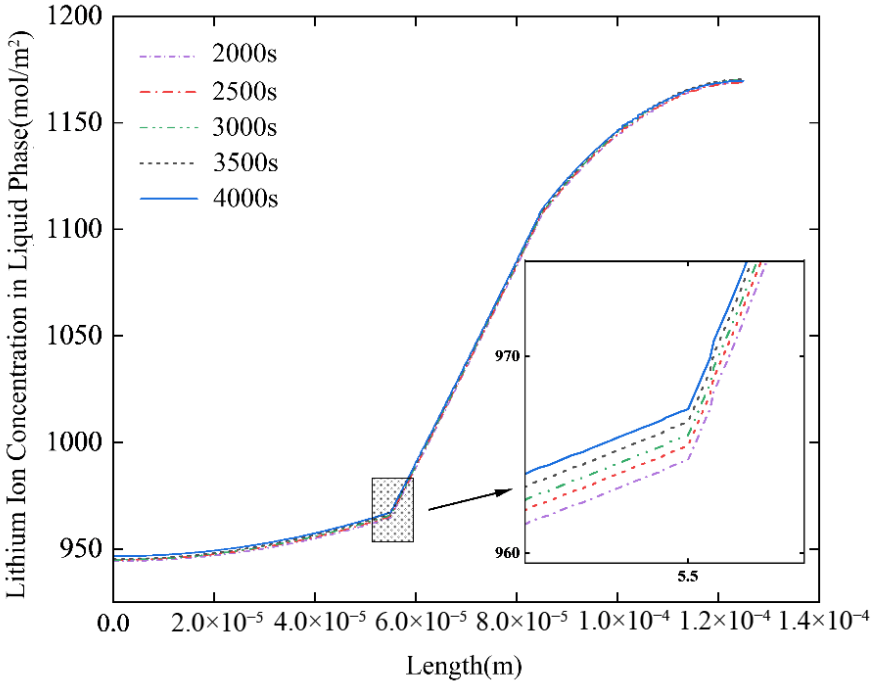

Figure 17. Lithium ion concentration profile in liquid phase.

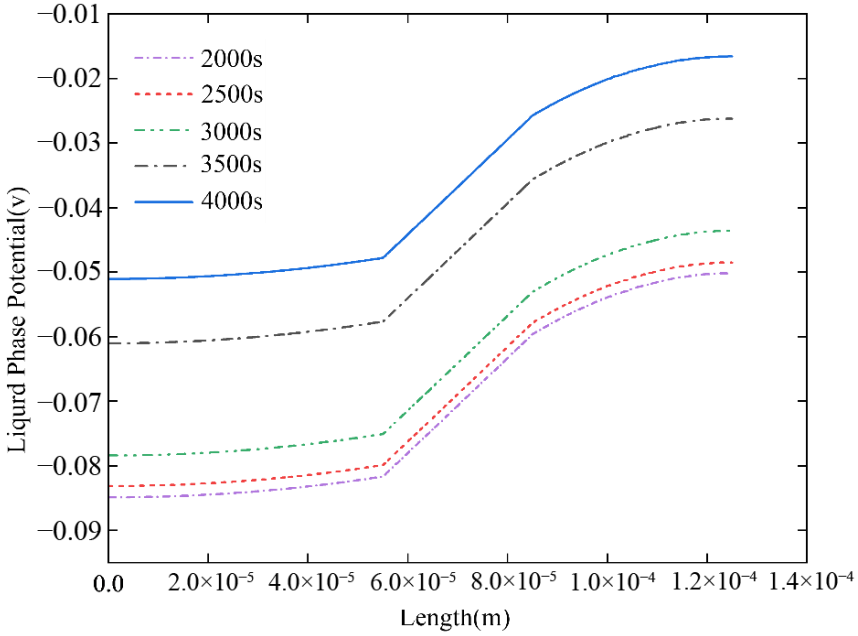

Figure 18. Liquid phase lithium-ion potential distribution diagram.

(3) Solid-phase Species and Potential Distribution

Figure 19 illustrates the distribution of solid-phase lithium-ion concentration over simulation time, while Figure 20 depicts the distribution of solid-phase lithium-ion potential over simulation time. From the observed trends in the solid-phase lithium-ion concentration and potential at the anode graphite on the left side of both figures, it is evident that, as charging time progresses, both the concentration and potential increase in a regular pattern, with the concentration at the right end being slightly higher than at the left. However, the overall change in potential is minor, only on the order of 10^{-5}, primarily due to the relatively high solid-phase conductivity.

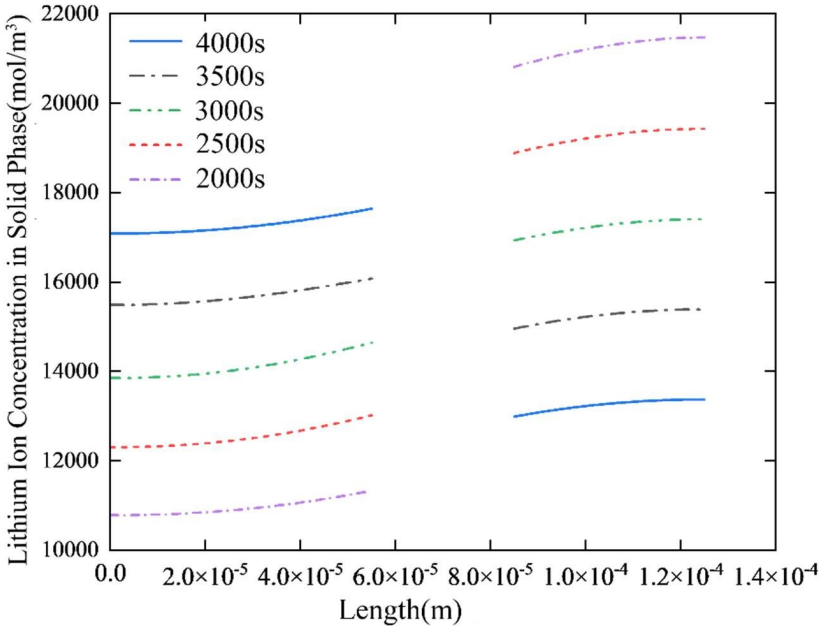

Figure 19. Solid phase lithium-ion concentration profile.

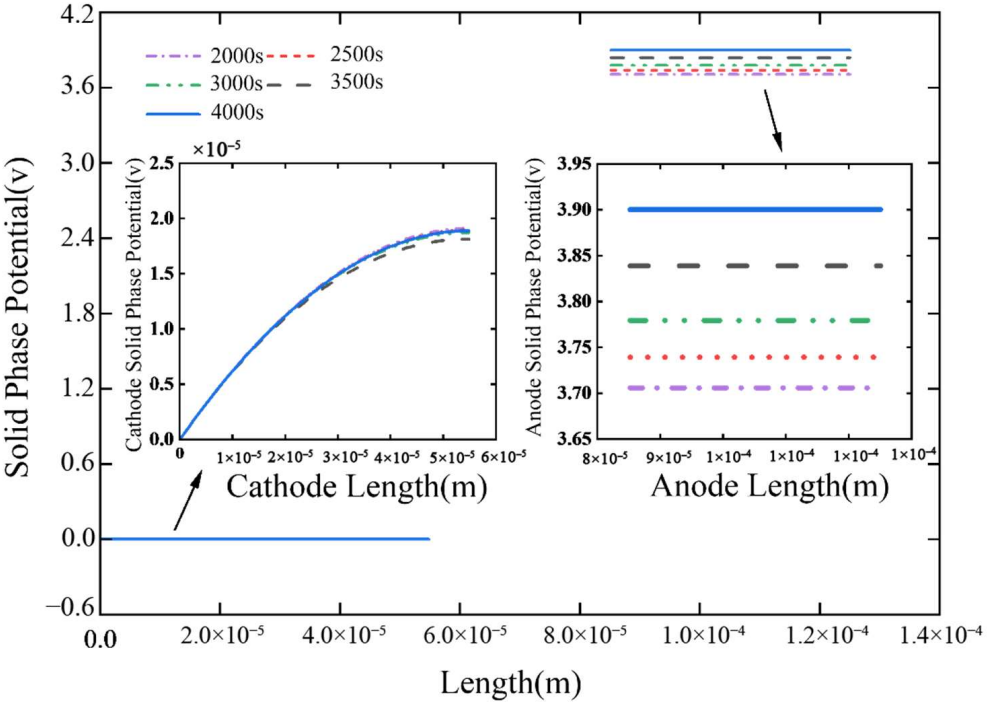

Figure 20. Solid phase lithium-ion potential distribution diagram.

The simulation results of various aspects of the aforementioned P2D model demonstrate that it can accurately represent the distribution of key parameters such as lithium-ion concentration and potential within the battery over the course of the simulation. Additionally, it can couple the battery capacity degradation caused by SEI film growth with the P2D model through the side reaction mechanism. Subsequently, the simplified P2D model proposed by Sarmadian et al. [43] was used to analyze the simplified conditions. The simplified variables were then substituted into the side reaction equations, resulting in the battery life objective function:

$$j_{\mathrm{SEI}}(x,t) = -i_{0,\mathrm{SEI}} \exp\left(\frac{F(U_m^{ref}(\theta_{m.\mathrm{avg}}) - U_{\mathrm{SEI}}^{ref}}{2RT}\right) \exp\left(-\mathrm{asinh}(\frac{-i}{2a_{\mathrm{ssa}} i_0 A l_{\mathrm{neg}}})\right). \quad (8)$$

Here, $U_m^{ref}(\theta_m(x,t))$ represents the function of the solid-phase material, and $\theta_{m.avg}$ denotes the average state of charge (SOC) of the solid-phase material.

4.2. Multi-Objective Optimization Case Study Analysis

In the aforementioned research, a detailed analysis was conducted with charging cost and battery life as optimization objectives. For pure electric vehicles, the multi-objective optimization concerning both charging cost and battery life can be expressed simultaneously. The expression for this multi-objective optimization is as follows:

$$\min_{P_{EV}} f_1 = \int_{t_e}^{t_s} f_{ele}(t, P_{EV})dt \quad (9)$$

$$\min_{P_{EV}} f_2 = \int_{t_e}^{t_s} \delta_{film}(SOC(t), P_{EV})dt \quad (10)$$

In this multi-objective optimization expression, f_1 represents the optimization of charging costs, while f_2 represents the optimization of battery capacity degradation. It can be seen that both objectives are achieved through the control of the decision variable, the charging curve of the pure electric vehicle. The constraints for the above-mentioned multi-objective optimization problem are as follows:

$$\int_{t_e}^{t_s} P_{EV}dt = D(n). \quad (11)$$

The preceding research results were thoroughly analyzed with a focus on optimizing charging cost and battery life. This section includes a simulation analysis based on a 20% penetration rate scenario, aimed at optimizing the charging efficiency of pure electric vehicles using a multi-objective genetic algorithm. The specific steps involved are as follows: (1) Statistically analyzing basic information such as daily driving distance, initial charging time, required charging amount, and charging duration for pure electric vehicle users using the Monte Carlo random sampling method. To minimize individual differences, the daily driving distance was uniformly set to 30 km, while the initial charging time and charging duration followed the valley-filling time demand. The required charging amount was set to 10.0 kW·h. Then, we set the information such as the number of individuals in the community and the number of iterations, where the number of communities is 120 and the number of iterations is 35. (2) Generating multiple feasible solutions for the pure electric vehicle charging curve $P_{EV}(t,n)$ as the initial parent population for the multi-objective optimization problem, with a loop count variable set to track the final genetic generations. (3) The fitness values of each individual are calculated based on the constraint conditions of the multi-objective optimization problem in Equation (11). (4) All individuals in the initial parent cohort were coded and subjected to genetic operator operations at set crossover and variance probabilities of 0.9 and 0.05, respectively. (5) Selecting superior individuals from the

initial parent population to form a new generation of parents. (6) Repeating steps 3–5 until the specified number of genetic iterations is reached, completing the evolution process.

Following the definition of the multi-objective optimization model for pure electric vehicle charging efficiency and the subsequent analysis, a simulation was conducted. All simulations were performed using Matlab 2022a on a personal computer with a 2.90 GHz CPU and 32 GB of memory. The Pareto optimal solution curve for the multi-objective optimization model, considering charging costs and battery capacity degradation of the electric vehicle, is shown in Figure 21.

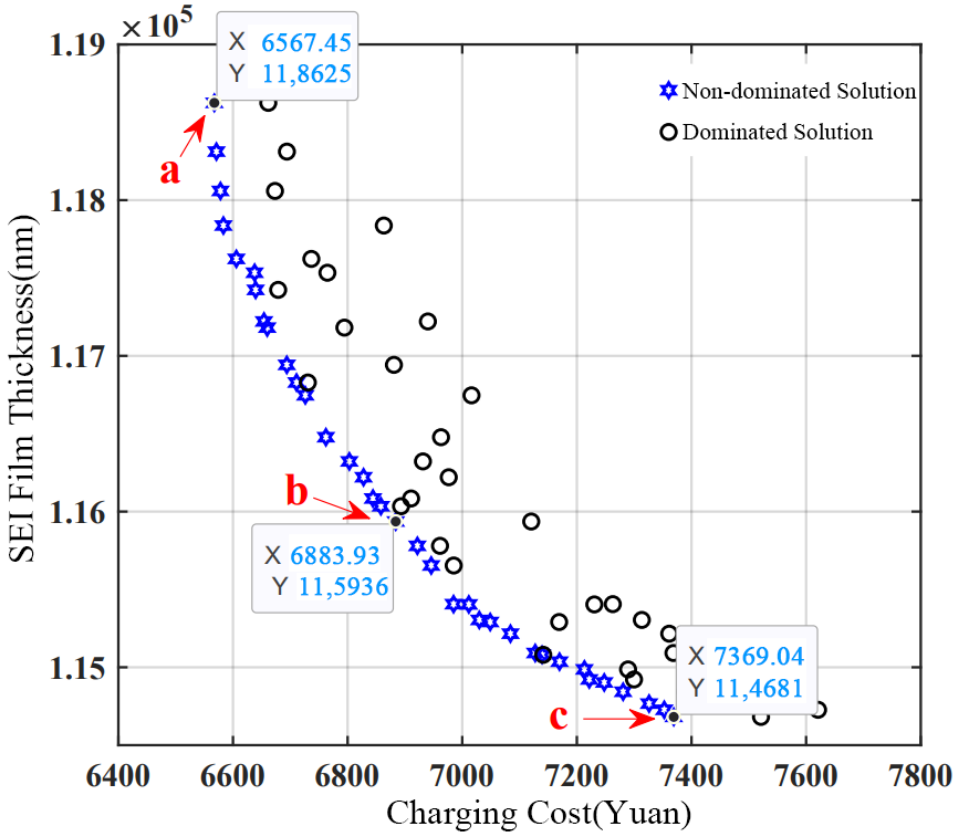

Figure 21. Pareto analysis of multi-objective optimization problems for pure electric vehicles.

The Figure 21 shows the Pareto front obtained after 35 iterations of the multi-objective genetic algorithm, illustrating the trade-off between charging costs and SEI film thickness. Each non-dominated solution in the figure represents a charging curve $P_{EV}(t,n)$. Among them, three representative non-dominated solutions, labeled a, b, and c, were selected. Solution A focuses on minimizing charging costs, Solution B balances both objectives, and Solution C prioritizes battery lifespan. To more intuitively illustrate the trend between the two optimization objectives in these three different non-dominated solutions, Table 3 provides a quantitative description of the charging costs and SEI film thickness for each solution.

Table 3. The value of each control solution in the multi-objective optimization scheme.

Optimization Goals \ Non-Dominated Solution	a	b	c
Charging Cost (yuan)	6567.5	6883.9	7369.0
SEI Film Thickness Values (nm)	118,625	115,936	114,681

According to Table 3, the Pareto front reflects the trade-off relationship between the two optimization objectives. Each Pareto solution corresponds to a different charging curve PEV for the electric vehicle, and due to varying objective weights, the charging curve will change depending on which objective is prioritized. By separately invoking the charging power curves of the three non-dominated solutions in the simulation program, the results are shown in Figure 22.

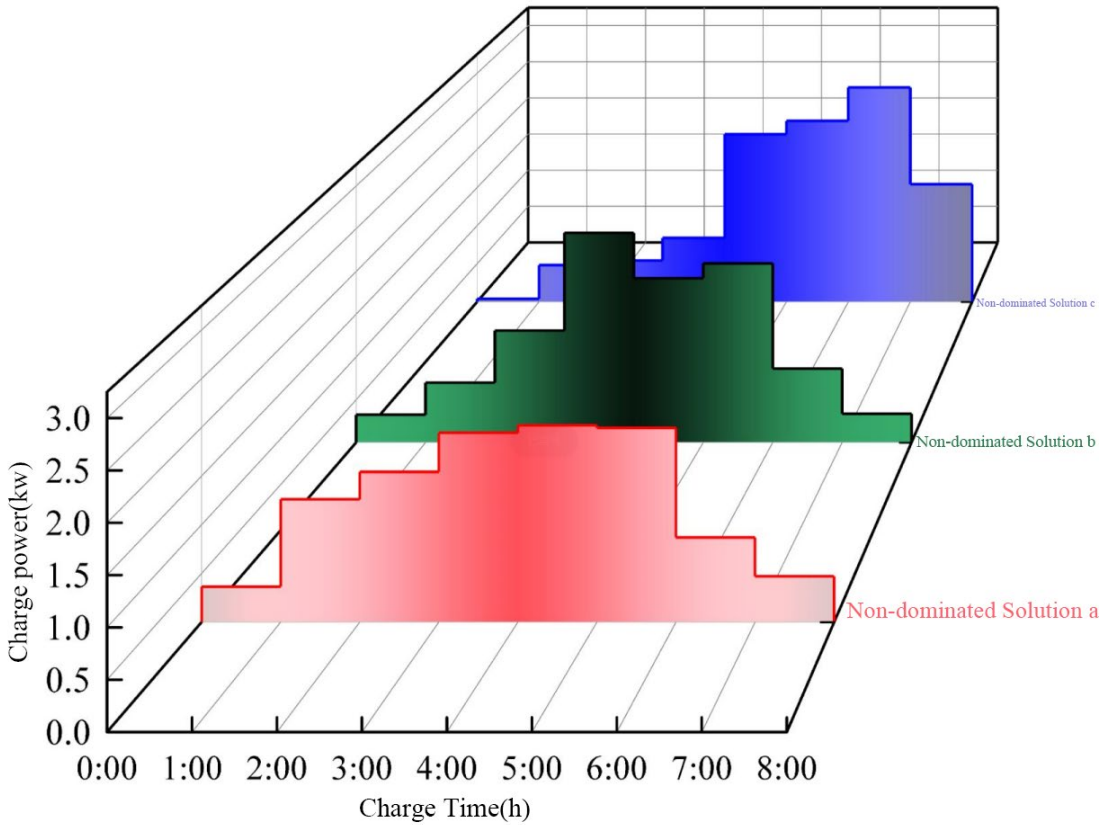

Figure 22. Charging power curves of three multi-objective optimization schemes.

The figure shows that the charging curves of the non-dominated solutions vary due to the differences in optimization weights. Among them, the non-dominated solution "a" represents the optimal scheme for minimizing charging costs, where the charging power remains relatively stable across all time periods during valley filling. Non-dominated solution "c" focuses on maximizing battery life, with lower charging power during the early stages of valley filling and higher power in the later stages. Non-dominated solution "b" strikes a balance between charging cost and battery life, primarily using high charging power in the mid-to-late stages of valley filling.

This paper uses non-dominated Solution B as an example to simulate the grid load profile under a 20% penetration rate, as shown in Figure 23. The figure indicates that non-dominated Solution B considers both charging cost and battery life as optimization objectives. As a result, its charging power is primarily concentrated between 3:00 and 6:00 the next day. In comparison to non-dominated Solution A, which evenly distributes charging power across all time periods to minimize charging costs, and non-dominated Solution C, which utilizes high power to reduce battery capacity degradation during the latter part of the valley period to achieve optimal battery life, Solution B offers a more balanced approach. This affords electric vehicle users greater flexibility in selecting charging curves.

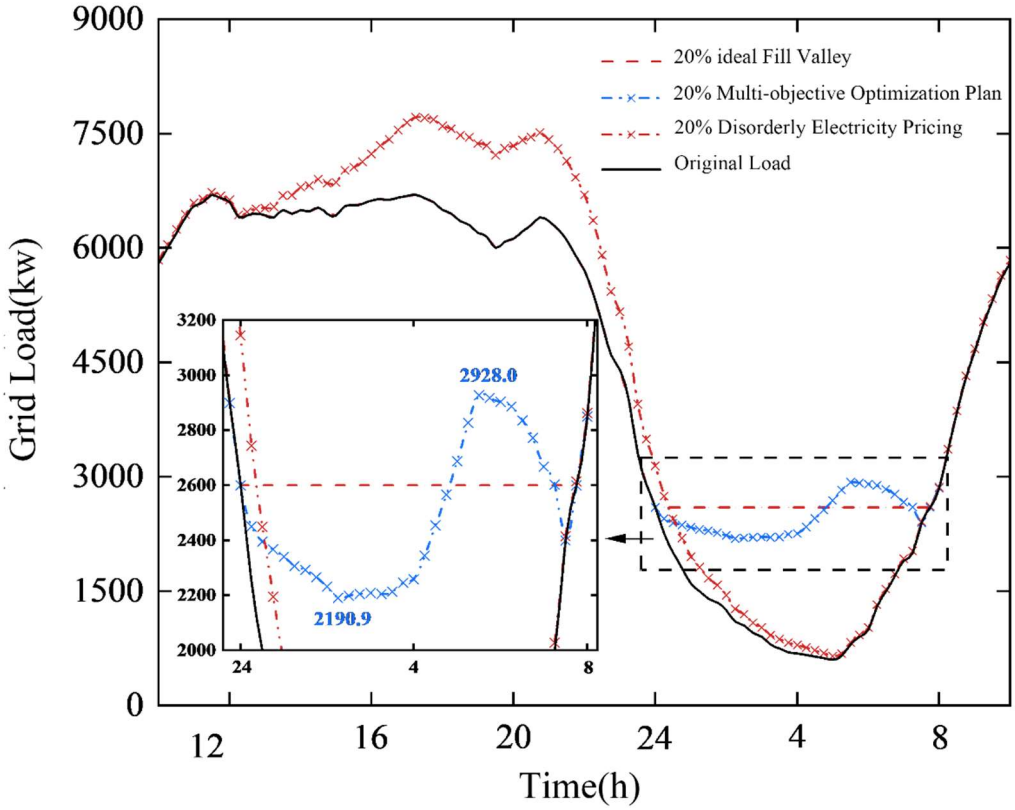

Figure 23. Visualization of the valley filling effect in multi-objective optimization solutions.

4.3. Analysis of the Impact of Optimization Error

To provide a clearer illustration of the differences in the total charging load of pure electric vehicles under a multi-objective optimization scheme and the ideal valley-filling state, an analysis of the average reaction rate of side reactions at different charging rates and battery state of charge (SOC) was conducted based on the P2D model of lithium-ion batteries, resulting in Figure 24. The figure revealed that the average reaction rate of side reactions follows a consistent trend across different charging rates. Specifically, when the SOC of the ternary lithium battery is between 0% and 80%, the average reaction rate of side reactions remains relatively low with minimal variation. However, when the SOC is between 80% and 100%, the average reaction rate increases dramatically, leading to accelerated battery capacity degradation and a rapid increase in solid electrolyte interphase (SEI) film thickness. To prioritize battery life in the optimization process, electric vehicle charging should maintain the battery at a lower SOC state. This indicates that the multi-objective optimization scheme necessitates charging at a lower power during the early to mid-valley periods and at a higher power during the later period. Consequently, this approach results in lower charging loads in the early to mid-periods, causing fluctuating impacts on the grid load under the multi-objective optimization scheme.

In essence, to effectively balance both optimization objectives, it is important for electric vehicle charging efficiency to maintain a lower state of charge (SOC) during the early to mid-valley periods, even though this may lead to some discrepancies in the grid's valley-filling effect. An analysis of the impact of the multi-objective optimization scheme on grid performance is conducted using quantitative indicators such as peak-to-valley difference ratio, load factor, and grid profit, as detailed in Table 4.

As shown in Figure 4, the data presented in the table illustrate that the multi-objective optimization scheme, designed to balance battery life and charging costs, leads to a 24.34% decrease in the peak-to-valley difference ratio compared to the unordered scheme. Furthermore, it decreases the generation cost of the charging load by 29.5%, lowers charging costs by 23.9%, and increases grid profits by 45.8%. Consequently, the multi-objective

optimization scheme enhances the charging efficiency for both the grid and electric vehicles. To verify the authenticity of the experimental results, this study compared the data from specialized studies [44–46] and found the results to be similar to those of this study.

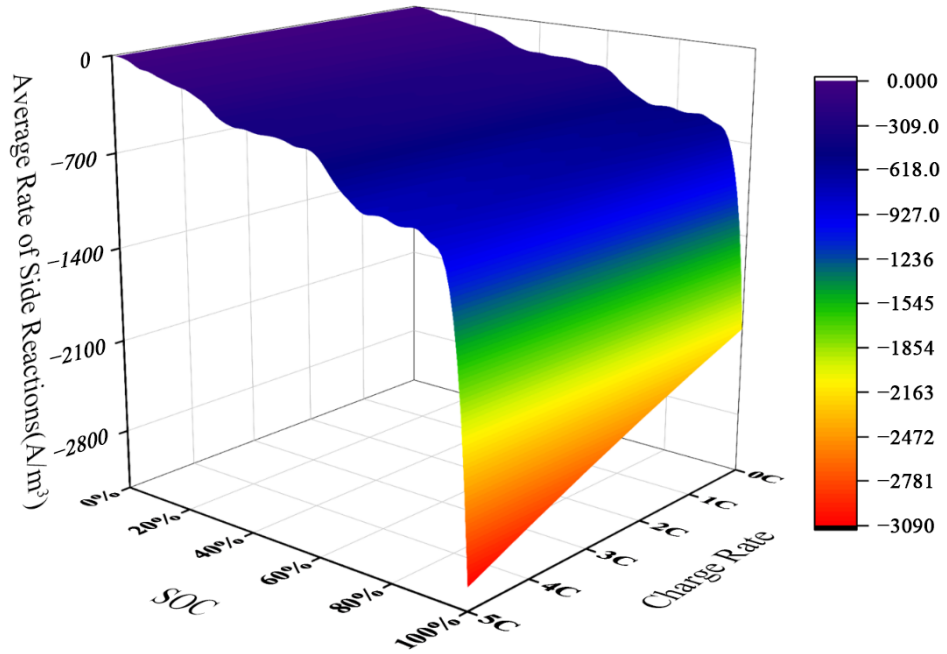

Figure 24. Relationship between average rate of side reactions, charging rate, and state of charge (SOC).

Table 4. Quantitative analysis of multi-objective optimization schemes.

Type	Peak-to-Valley Difference/kW	Peak-to-Valley Spread/%	Load Factor/%	Charging Load Power Generation Cost/¥	Charging Cost/¥	Grid Profit/¥
20%—disorderly tariffs	7073.7	91.64	64.71	8377.38	9049.95	672.57
20%—Multi-objective optimization	4509.1	67.30	70.72	5903.00	6883.90	980.90

5. Conclusions

This research paper addresses the issue of negative impacts on grid system performance caused by uncoordinated charging loads in large-scale EV charging programs. It aims to optimize charging efficiency by employing a multi-objective genetic algorithm to balance charging costs and battery life, leading to Pareto optimal solutions in the form of a set of charging curves. These results are crucial for both charging efficiency and grid operation performance. The key findings are as follows:

(1) The study utilizes a probability density model and the Monte Carlo random sampling method to predict the total charging load for EVs. Simulations conducted using Matlab 2022a show that peak loads occur at 20:00, specifically at 1784.4 kW, 1220.7 kW, and 615.5 kW for different quantities of EVs. These peak loads coincide with the original grid load peak, indicating an inevitable impact on the grid's operational performance.

(2) Based on the IEEE33-node distribution network system, three EV penetration schemes were simulated to analyze the impact of uncoordinated charging loads on the grid. Evaluation indicators such as the peak-to-valley difference ratio and node voltage were defined, demonstrating that as penetration rates increase, the peak-to-valley difference ratio also increases, and the load rate decreases. Additionally, the minimum node voltages for the three schemes—0.924 pu, 0.912 pu, and 0.896 pu—were all below the specified range, severely affecting the charging efficiency and economic viability of EVs.

(3) Based on the research into the impact of uncoordinated charging on the grid, a multi-objective optimization function was constructed focusing on charging costs and battery life. Using a multi-objective genetic algorithm, Pareto fronts were obtained in the form of charging curves under different optimization weights. Taking the example of a 20% penetration rate with both optimization objectives considered, simulations were conducted to evaluate the valley-filling effect on the grid, analyze the causes of errors, and quantify the results of the multi-objective optimization scheme. The study results indicate that, compared to the uncoordinated scheme, the multi-objective optimization scheme reduces the peak-to-valley difference ratio by 24.34%, decreases the generation cost of the charging load by 29.5%, lowers charging costs by 23.9%, and increases grid profits by 45.8%, further optimizing EV charging efficiency.

Author Contributions: Conceptualization, H.X.; software, H.X., Z.L. and F.J.; formal analysis, H.X., F.J. and Z.L.; investigation, H.X., Z.L., F.J., Q.M., J.H. and J.Z.; resources, H.X.; writing—original draft preparation, H.X., Z.L. and F.J.; writing—review and editing, H.X., Z.L., F.J., Q.M., J.H. and J.Z.; supervision, H.X.; funding acquisition, H.X., F.J., Q.M. and J.H. All authors have read and agreed to the published version of the manuscript.

Funding: This work is supported by the 2023 Guangxi Educational Science Planning Project, with project number 2023A071.

Data Availability Statement: All data used to support the findings of this study are included within the article.

Conflicts of Interest: The authors declare that there are no conflicts of interest regarding the publication of this paper.

Nomenclature

δ_s	The expected average daily driving range of pure electric vehicles
σ_t	The variance
X	The specific kilometers driven (km)
t_0	The starting charging time for pure electric vehicles (h)
$SOC_{\text{pre.t}}$	The battery status value at the start of charging (kW·h)
t	The charging time (h)
E_d	The 100 km power consumption of pure electric vehicle (kW·h)
D_n	The amount of EV to be charged (kW·h)
B	The battery capacity (kW·h)
P_c	The charging power for pure electric vehicles (kW/h)
K	The charging constant
σ	The Grid Peak-Valley Difference Ratio
ρ	The grid load factor
P_{peak}	The peak load during a defined time period (kW)
P_{avg}	The average load over a defined period of time (kW)
A	The cross-sectional area of graphite material
a_a	The anode electrochemical transfer reaction coefficient
a_c	The cathode chemical transfer reaction coefficient
a_{ssa}	The specific surface area of active particulate material
Ds	The solid-phase diffusion coefficient
D_l	The liquid phase diffusion coefficient
F_{EV}	The charging costs
f_{ele}	The optimal time-sharing tariff
$i_{0,SEI}$	The SEI membrane side reaction exchange current density
$j_{SEI(x,t)}$	The side-reaction current density
N	The number of pure electric vehicles
$P_{EV(t,n)}$	The charging power curve
$P_{EV.sum}$	The sum of charging power curves
P_{valley}	The valley load

$P_{v\text{-}f}$	The height of valley filling load
R	The ideal gas constant
T	The temperature
$t_{ev,s}$	The starting time of charging for pure electric vehicles
$t_{ev,e}$	The end-of-charge time for pure electric vehicles

References

1. Olale, E.; Ochuodho, T.O.; Lantz, V.; El Armali, J. The environmental Kuznets curve model for greenhouse gas emissions in Canada. *J. Clean. Prod.* **2018**, *184*, 859–868. [CrossRef]
2. Rahman, S.M.A.; Rizwanul Fattah, I.M.; Ong, H.C.; Zamri, M.F.M.A. State-of-the-Art of Strategies to Reduce Exhaust Emissions from Diesel Engine Vehicles. *Energies* **2021**, *14*, 1766. [CrossRef]
3. Ni, P.; Wang, X.; Li, H. A review on regulations, current status, effects and reduction strategies of emissions for marine diesel engines. *Fuel* **2020**, *279*, 118477. [CrossRef]
4. Cai, T.; Zhao, D. Effects of fuel composition and wall thermal conductivity on thermal and NOx emission performances of an ammonia/hydrogen-oxygen micro-power system. *Fuel Process. Technol.* **2020**, *209*, 106527. [CrossRef]
5. He, H.; Sun, F.; Wang, Z.; Lin, C.; Zhang, C.; Xiong, R.; Deng, J.; Zhu, X.; Xie, P.; Zhang, S. China's battery electric vehicles lead the world: Achievements in technology system architecture and technological breakthroughs. *Green Energy Intell. Transp.* **2022**, *1*, 100020. [CrossRef]
6. Sorlei, I.-S.; Bizon, N.; Thounthong, P.; Varlam, M.; Carcadea, E.; Culcer, M.; Iliescu, M.; Raceanu, M. Fuel cell electric vehicles—A brief review of current topologies and energy management strategies. *Energies* **2021**, *14*, 252. [CrossRef]
7. Selvakumar, S.G. Electric and Hybrid Vehicles—A Comprehensive Overview. In Proceedings of the 2021 IEEE 2nd International Conference on Electrical Power and Energy Systems (ICEPES), Bhopal, India, 10–11 December 2021; pp. 1–6.
8. Zhang, Z.; Zhong, W.; Tan, D.; Cui, S.; Pan, M.; Zhao, Z.; Zhang, J.; Hu, J. Hydrocarbon adsorption mechanism of modern automobile engines and methods of reducing hydrocarbon emissions during cold start process: A review. *J. Environ. Manag.* **2024**, *353*, 120188. [CrossRef] [PubMed]
9. Wang, H.; Guo, J. Research on the impact mechanism of multiple environmental regulations on carbon emissions under the perspective of carbon peaking pressure: A case study of China's coastal regions. *Ocean Coast. Manag.* **2024**, *249*, 106985. [CrossRef]
10. Goh, H.H.; Zong, L.; Zhang, D.; Liu, H.; Dai, W.; Lim, C.S.; Kurniawan, T.A.; Teo, K.T.K.; Goh, K.C. Mid-and long-term strategy based on electric vehicle charging unpredictability and ownership estimation. *Int. J. Electr. Power Energy Syst.* **2022**, *142*, 108240. [CrossRef]
11. Karki, A.; Phuyal, S.; Tuladhar, D.; Basnet, S.; Shrestha, B.P. Status of pure electric vehicle power train technology and future prospects. *Appl. Syst. Innov.* **2020**, *3*, 35. [CrossRef]
12. Zhang, Q.; Wang, L.; Li, G.; Liu, Y. A real-time energy management control strategy for battery and supercapacitor hybrid energy storage systems of pure electric vehicles. *J. Energy Storage* **2020**, *31*, 101721. [CrossRef]
13. Xu, Y.; Zhang, H.; Yang, Y.; Zhang, J.; Yang, F.; Yan, D.; Yang, H.; Wang, Y. Optimization of energy management strategy for extended range electric vehicles using multi-island genetic algorithm. *J. Energy Storage* **2023**, *61*, 106802. [CrossRef]
14. Yi, Z.; Scoffield, D.; Smart, J.; Meintz, A.; Jun, M.; Mohanpurkar, M.; Medam, A. A highly efficient control framework for centralized residential charging coordination of large electric vehicle populations. *Int. J. Electr. Power Energy Syst.* **2020**, *117*, 105661. [CrossRef]
15. Yi, T.; Zhang, C.; Lin, T.; Liu, J. Research on the spatial-temporal distribution of electric vehicle charging load demand: A case study in China. *J. Clean. Prod.* **2020**, *242*, 118457. [CrossRef]
16. Xing, Y.; Li, F.; Sun, K.; Wang, D.; Chen, T.; Zhang, Z. Multi-type electric vehicle load prediction based on Monte Carlo simulation. *Energy Rep.* **2022**, *8*, 966–972. [CrossRef]
17. Polat, Ö.; Eyüboğlu, O.H.; Gül, Ö. Monte Carlo simulation of electric vehicle loads respect to return home from work and impacts to the low voltage side of distribution network. *Electr. Eng.* **2020**, *103*, 439–445. [CrossRef]
18. Bian, H.; Guo, Z.; Zhou, C.; Peng, S. Multi-time scale electric vehicle charging load forecasting considering constant current charging and parallel computing. *Energy Rep.* **2022**, *8*, 722–732. [CrossRef]
19. Liu, L.; Zhang, Y.; Da, C.; Huang, Z.; Wang, M. Optimal allocation of distributed generation and electric vehicle charging stations based on intelligent algorithm and bi-level programming. *Int. Trans. Electr. Energy Syst.* **2020**, *30*, e12366. [CrossRef]
20. Wang, Z.H.; Fan, S.X.; Liu, B.Z.; Liu, X.W.; Wei, Z.C. Coordinated charging strategy of plug-in electric vehicles for maximising the distributed energy based on time and location. *J. Eng.* **2018**, *2017*, 1740–1744. [CrossRef]
21. Dolatabadi, S.H.; Ghorbanian, M.; Siano, P.; Hatziargyriou, N.D. An Enhanced IEEE 33 Bus Benchmark Test System for Distribution System Studies. *IEEE Trans. Power Syst.* **2021**, *36*, 2565–2572. [CrossRef]
22. Zhu, J.; Yang, Z.; Mourshed, M.; Guo, Y.; Zhou, Y.; Chang, Y.; Wei, Y.; Feng, S. Electric vehicle charging load forecasting: A comparative study of deep learning approaches. *Energies* **2019**, *12*, 2692. [CrossRef]
23. Ahmad, N.; Ghadi, Y.; Adnan, M.; Ali, M. Load forecasting techniques for power system: Research challenges and survey. *IEEE Access* **2022**, *10*, 71054–71090. [CrossRef]
24. Habib, S.; Khan, M.M.; Abbas, F.; Ali, A.; Hashmi, K.; Shahid, M.U.; Bo, Q.; Tang, H. Risk evaluation of distribution networks considering residential load forecasting with stochastic modeling of electric vehicles. *Energy Technol.* **2019**, *7*, 1900191. [CrossRef]

25. Nour, M.; Chaves-Ávila, J.P.; Magdy, G.; Sánchez-Miralles, Á. Review of Positive and Negative Impacts of Electric Vehicles Charging on Electric Power Systems. *Energies* **2020**, *13*, 4675. [CrossRef]
26. Muttaqi, K.M.; Isac, E.; Mandal, A.; Sutanto, D.; Akter, S. Fast and random charging of electric vehicles and its impacts: State-of-the-art technologies and case studies. *Electr. Power Syst. Res.* **2024**, *226*, 109899. [CrossRef]
27. Sadeghian, O.; Oshnoei, A.; Mohammadi-Ivatloo, B.; Vahidinasab, V.; Anvari-Moghaddam, A. A comprehensive review on electric vehicles smart charging: Solutions, strategies, technologies, and challenges. *J. Energy Storage* **2022**, *54*, 105241. [CrossRef]
28. Sanguesa, J.A.; Torres-Sanz, V.; Garrido, P.; Martinez, F.J.; Marquez-Barja, J.M. A review on electric vehicles: Technologies and challenges. *Smart Cities* **2021**, *4*, 372–404. [CrossRef]
29. Tran, M.-K.; Bhatti, A.; Vrolyk, R.; Wong, D.; Panchal, S.; Fowler, M.; Fraser, R. A review of range extenders in battery electric vehicles: Current progress and future perspectives. *World Electr. Veh. J.* **2021**, *12*, 54. [CrossRef]
30. Wang, X.; Renne, J.L. Socioeconomics of Urban Travel in the US: Evidence from the 2017 NHTS. *Transp. Res. Part D Transp. Environ.* **2023**, *116*, 103622. [CrossRef]
31. Das, S.; Acharjee, P.; Bhattacharya, A. Charging scheduling of electric vehicle incorporating grid-to-vehicle and vehicle-to-grid technology considering in smart grid. *IEEE Trans. Ind. Appl.* **2020**, *57*, 1688–1702. [CrossRef]
32. Hannan, M.; Mollik, M.; Al-Shetwi, A.Q.; Rahman, S.; Mansor, M.; Begum, R.; Muttaqi, K.; Dong, Z. Vehicle to grid connected technologies and charging strategies: Operation, control, issues and recommendations. *J. Clean. Prod.* **2022**, *339*, 130587. [CrossRef]
33. Feng, J.; Chang, X.; Fan, Y.; Luo, W. Electric vehicle charging load prediction model considering traffic conditions and temperature. *Processes* **2023**, *11*, 2256. [CrossRef]
34. Li, N.; Hakvoort, R.A.; Lukszo, Z. Segmented energy tariff design for flattening load demand profile. In Proceedings of the 2020 IEEE PES Innovative Smart Grid Technologies Europe (ISGT-Europe), The Hague, The Netherlands, 26–28 October 2020; pp. 849–853.
35. *GB/T 12305-2008*; Power Quality-Deviation of Supply Voltage. Standardization Administration of China: Beijing, China, 2008.
36. Amin, A.; Tareen, W.U.K.; Usman, M.; Ali, H.; Bari, I.; Horan, B.; Mekhilef, S.; Asif, M.; Ahmed, S.; Mahmood, A. A review of optimal charging strategy for electric vehicles under dynamic pricing schemes in the distribution charging network. *Sustainability* **2020**, *12*, 10160. [CrossRef]
37. Hussain, S.; Thakur, S.; Shukla, S.; Breslin, J.G.; Jan, Q.; Khan, F.; Ahmad, I.; Marzband, M.; Madden, M.G. A heuristic charging cost optimization algorithm for residential charging of electric vehicles. *Energies* **2022**, *15*, 1304. [CrossRef]
38. Zhou, G.; Zhu, Z.; Luo, S. Location optimization of electric vehicle charging stations: Based on cost model and genetic algorithm. *Energy* **2022**, *247*, 123437. [CrossRef]
39. Ekatpure, R. Optimizing Battery Lifespan and Performance in Electric Vehicles through Intelligent Battery Management Systems. *J. Sustain. Urban Futures* **2024**, *14*, 11–28.
40. Thakur, A.K.; Sathyamurthy, R.; Velraj, R.; Saidur, R.; Pandey, A.; Ma, Z.; Singh, P.; Hazra, S.K.; Sharshir, S.W.; Prabakaran, R. A state-of-the art review on advancing battery thermal management systems for fast-charging. *Appl. Therm. Eng.* **2023**, *226*, 120303. [CrossRef]
41. Zadeh, P.G.; Gholamalizadeh, E.; Wang, Y.; Chung, J.D. Electrochemical modeling of a thermal management system for cylindrical lithium-ion battery pack considering battery capacity fade. *Case Stud. Therm. Eng.* **2022**, *32*, 101878. [CrossRef]
42. Rufino Júnior, C.A.; Sanseverino, E.R.; Gallo, P.; Amaral, M.M.; Koch, D.; Kotak, Y.; Diel, S.; Walter, G.; Schweiger, H.-G.; Zanin, H. Unraveling the Degradation Mechanisms of Lithium-Ion Batteries. *Energies* **2024**, *17*, 3372. [CrossRef]
43. Sarmadian, A.; Widanage, W.D.; Shollock, B.; Restuccia, F. Experimentally-verified thermal-electrochemical simulations of a cylindrical battery using physics-based, simplified and generalised lumped models. *J. Energy Storage* **2023**, *70*, 107910. [CrossRef]
44. Jin, C.; Tang, J.; Ghosh, P. Optimizing Electric Vehicle Charging: A Customer's Perspective. *IEEE Trans. Veh. Technol.* **2013**, *62*, 2919–2927. [CrossRef]
45. Chupradit, S.; Widjaja, G.; Mahendra, S.; Ali, M.; Tashtoush, M.; Surendar, A.; Kadhim, M.; Oudah, A.; Fardeeva, I.; Firman, F. Modeling and Optimizing the Charge of Electric Vehicles with Genetic Algorithm in the Presence of Renewable Energy Sources. *J. Oper. Autom. Power Eng.* **2023**, *11*, 33–38.
46. Qin, L.; Yujiao, L.; Shi, X.; Shi, F. Study on Coordinated Charging Strategy for Electric Vehicles Based on Genetic Algorithm. In Proceedings of the 2020 IEEE/IAS Industrial and Commercial Power System Asia (I&CPS Asia), Weihai, China, 13–15 July 2020; pp. 1523–1527.